การสังเคราะห์ การพิสูจน์เอกลักษณ์และฤทธิ์ต้านมะเร็งของแอนโดรกราโฟไลด์ซักซิเนต
กราฟต์บนไคโตซาน

นางสาวศิวพร ศรีมงคล

วิทยานิพนธ์นี้เป็นส่วนหนึ่งของการศึกษาตามหลักสูตรปริญญาวิทยาศาสตรมหาบัณฑิต
สาขาวิชาปิโตรเคมีและวิทยาศาสตร์พอลิเมอร์
คณะวิทยาศาสตร์ จุฬาลงกรณ์มหาวิทยาลัย
ปีการศึกษา 2555
ลิขสิทธิ์ของจุฬาลงกรณ์มหาวิทยาลัย

SYNTHESIS, CHARACTERIZATION AND ANTICANCER ACTIVITY OF
ANDROGRAPHOLIDESUCCINATE GRAFTED CHITOSAN

Miss Siwaporn Srimongkol

A Thesis Submitted in Partial Fulfillment of the Requirements
for the Degree of Master of Science Program in Petrochemistry and Polymer Science
Faculty of Science
Chulalongkorn University
Academic Year 2012
Copyright of Chulalongkorn University

Thesis Title	SYNTHESIS, CHARACTERIZATION AND ANTICANCER ACTIVITY OF ANDROGRAPHOLIDESUCCINATE GRAFTED CHITOSAN
By	Miss Siwaporn Srimongkol
Field of Study	Petrochemistry and Polymer Science
Thesis Advisor	Assistant Professor Pattara Sawasdee, Ph.D.

Accepted by the Faculty of Science, Chulalongkorn University in Partial Fulfillment of the Requirements for the Master's Degree

.... Dean of the Faculty of Science

(Professor Supot Hannongbua, Dr.rer.nat.)

THESIS COMMITTEE

.... Chairman

(Assistant Professor Warinthorn Chavasiri, Ph.D.)

.... Thesis Advisor

(Assistant Professor Pattara Sawasdee, Ph.D.)

.... Examiner

(Associate Professor Nuanphun Chantarasiri, Ph.D.)

.... External Examiner

(Assistant Professor Boon-ek Yingyongnarongkul, Ph.D.)

ศิวพร ศรีมงคล : การสังเคราะห์ การพิสูจน์เอกลักษณ์และฤทธิ์ต้านมะเร็งของแอนโดรกรา
โฟไลด์ซักซิเนตกราฟต์บนไคโตซาน (SYNTHESIS, CHARACTERIZATION AND
ANTICANCER ACTIVITY OF ANDROGRAPHOLIDESUCCINATE GRAFTED
CHITOSAN) อ.ที่ปรึกษาวิทยานิพนธ์หลัก : ผศ. ดร.พัฒทรา สวัสดี, 70 หน้า.

อนุพันธ์ของไคโตซานชนิดใหม่ (แอนโดรกราโฟไลด์ซักซิเนตกราฟต์บนไคโตซาน) เตรียม
ได้จากการกราฟต์แอนโดรกราโฟไลต์-14-แอลฟา-ซักซิเนตลงบนไคโตซาน ซึ่งแอนโดรกราโฟไลด์ซักซิ
เนตกราฟต์บนไคโตซานที่มีเปอร์เซ็นต์การแทนที่ 7.42 เปอร์เซ็นต์ได้รับการยืนยันโครงสร้างด้วย
เทคนิคโปรตอน เอ็นเอ็มอาร์และเทคนิคเอฟทีไออาร์ นอกจากนี้แอนโดรกราโฟไลด์ซักซิเนตกราฟต์
บนไคโตซานสามารถจัดเรียงตัวเป็นอนุภาคนาโนได้ในน้ำที่ความเข้มข้นวิกฤตเท่ากับ 0.063
มิลลิกรัม/มิลลิลิตร ซึ่งอนุภาคนี้มีลักษณะเป็นทรงกลมและมีเส้นผ่านศูนย์กลางเฉลี่ยเท่ากับ 154 ±
2 นาโนเมตร สมบัติความเป็นผลึกของแอนโดรกราโฟไลด์ซักซิเนตกราฟต์บนไคโตซานถูกศึกษาด้วย
เทคนิคเอ็กซ์อาร์ดี พบว่าสมบัติความเป็นผลึกของไคโตซานถูกเปลี่ยนเป็นอะมอร์ฟัสเมื่อถูกกราฟต์
ด้วยแอนโดรกราโฟไลต์-14-แอลฟา-ซักซิเนต และนอกจากนี้ยังพบว่าแอนโดรกราโฟไลด์ซักซิเนต
กราฟต์บนไคโตซานมีความเสถียรทางความร้อนต่ำกว่าไคโตซาน เนื่องจากแอนโดรกราโฟไลต์-14-
แอลฟา-ซักซิเนตเข้าไปแทรกอยู่ระหว่างสายโซ่ของไคโตซานที่อัดตัวกันแน่น แอนโดรกราโฟไลด์ซักซิ
เนตกราฟต์บนไคโตซานมีความเป็นพิษต่อเซลล์มะเร็งปากมดลูกและมะเร็งเต้านมมากกว่าแอนโด
รกราโฟไลด์ในการวิเคราะห์เอ็มทีที

5372343823 : MAJOR PETROCHEMISTRY AND POLYMER SCIENCE

KEYWORDS: ANDROGRAPHOLIDE / SELF-ASSEMBLY / CHITOSAN / NANOPARTICLES / ANTI-CANCER

SIWAPORN SRIMONGKOL: SYNTHESIS, CHARACTERIZATION AND ANTICANCER ACTIVITY OF ANDROGRAPHOLIDESUCCINATE GRAFTED CHITOSAN. ADVISOR: ASST. PROF. PATTARA SAWASDEE, Ph.D., 70 pp.

A new chitosan derivative, andrographolidesuccinate grafted chitosan (AGS-g-CS), is prepared by grafting andrographolide-14-α-O-succinate on the chitosan chain. The structure of AGS-g-CS with the degree of andrographolide-14-α-O-succinate substitution 7.42 % is confirmed through the ^{1}H NMR and FTIR analysis. Moreover, AGS-g-CS can self-assembled to be nanoparticles with the critical aggregation concentration of 0.063 mg/mL in the distilled water. These particles show spherical shapes with the average size of 154 ± 2 nm. The crystal property of AGS-g-CS is studied by XRD. The crystalline form of chitosan is changed to amorphous form when it was grafted with andrographolide-14-α-O-succinate. Moreover, AGS-g-CS has lower thermal stability than chitosan because andrographolide-14-α-O-succinate groups interfered with the close packing between chitosan chains. AGS-g-CS exhibit higher cytotoxicity than AG towards cervical and breast cancer cell lines in MTT assay.

Field of Study: <u>Petrochemistry and Polymer Science</u> Student's Signature......................

Academic Year: <u>   2012   </u> Advisor's Signature....................

ACKNOWLEDGEMENTS

CONTENTS

LIST OF TABLES

LIST OF FIGURES

Page

LIST OF SCHEMES

LIST OF ABBREVIATIONS

%	percentage
α	alpha
δ	chemical shift
AG	andrographolide
AGS-*g*-CS	andrographolidesuccinate grafted chitosan
ATR-IR	attenuated total reflectance-infrared
CAC	critical aggregation concentration
˚C	degree Celsius (centrigrade)
DLS	dynamic light scattering
DSC	differential Scanning Calorimeter
et al.	et alli, and other
FTIR	fourier transform infrared spectrophotometer
g	gram
h	hour
HPLC	high performance liquid chromatography
Hz	hertz
μL	microliter
M	molar
mg	milligram
mV	millivolt
min	minute
mL	milliliter
mM	millimolar
mmol	millimole
$\overline{M}_w$	molecular weight
nm	nanometer
NMR	nuclear magnetic resonance
NSCS	*N*-succinyl chitosan
PBS	phosphate buffer saline

PDI	polydispersity index
pH	power of hydrogen ion or the negative logarithm (base ten)
ppm	part per million
RT	room temperature
R_t	retention time
R_f	retention factor
ref	reference
rpm	round per minute
SD	standard deviation
SEM	scanning electron microscope
TGA	thermal gravimetric analysis
v/v	volume by volume
λ	wavelength
w/v	weight by volume
w/w	weight by weight
XRD	X-ray diffractometer

CHAPTER I

INTRODUCTION

1.1 Introduction

When the drug is ingested or injected into the body, the major amount of drug is metabolized by enzyme or pH in the body and broken down into inactive substances, or distributed over the normal tissues and organs. Whereas the amount of remaining drug reach the site of therapeutic action and the effective treatment is limited due to its low bioavailability [1]. Thus, the dosage and dosage frequency have to be increased to the patients [2]. Therefore, drug delivery system is used to solve this problem. This system is the process applied to ensure that the drug or pharmaceutical compound administer into the body and reach the therapeutic area. This technology benefits to improve drug efficiency, which is safe by reducing side effects, enhance bioavailability, control the drug release rate as well as reduce the frequency of drug therapy (prolong biological activity) [3-4]. The drug is incorporated into the carrier, which protects the drug from physical and chemical degradation, takes the drug to diseased organ and slowly releases to the active sites.

The types of carriers for drug delivery system are, for examples, liposomes, solid lipid nanoparticles, phytosomes, micro/nano emulsion, polymeric micro/nano particles, and dendrimers [5]. Each type shows different pharmacokinetics and pharmacodynamics of drugs [1]. However, in nowadays, the nano-sizes of carriers have received increasing attention. Nanocarriers are solid colloidal particles with diameter ranging from 1-1000 nm. Thus, they can pass through the smallest capillary vessels and avoid rapid removal by phagocytes resulting in their prolonged duration in blood stream. They can penetrate through cells and tissue gaps to achieve target organs. Moreover, the outstanding advantages of this system are showing controlled release properties, improving the utility of drugs and reducing toxic side effect [6].

Recently, many researchers have studied nanopolymeric particles used as the drug carriers because the polymer can be localized and controlled release of drugs

over a period of months [7]. Polymeric materials in drug delivery must be safe, biocompatible, biodegradable in human body and not cause excessive immune responses [8]. It can be both synthetic and natural polymers. Chitosan (Figure 1.1) is one of biodegradable polymer which has been commonly used for encapsulating drug and forming nanoparticles [9]. Chitosan is a natural polymer derived from chitin by exhaustive deacylation. It has many attractive properties such as bioactive, biocompatible and biodegradable properties resulting in the suitability for using in pharmaceutical and biomedical fields. Moreover, it is nontoxic substance for human body. However, chitosan is soluble in aqueous acidic medium (pH < 6.5) but insoluble in water due to strong intermolecular hydrogen bonding (H-bond) [10]. In order to improve its physicochemical and biological properties, several chemical modifications of chitosan have been reported [11-12]. The structure of chitosan contains three reactive functional groups per a glucosamine unit including two hydroxyl groups and one amino group [13], which can be modified by attaching hydrophobic or hydrophilic segments to chitosan backbone. This property makes it to be an attractive material for using in biomedical applications [14].
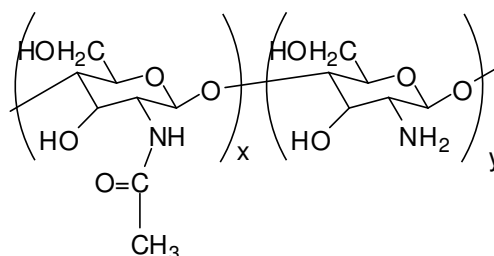
Figure 1.1 Chemical structure of chitosan

Many derivatives of chitosan have been synthesized and used as drug carriers, for examples, oleoyl-carboxymethyl chitosan (OCMCS) [15], cholic acid chitosan-*g*-mPEG [16] , chitosan-g-poly(β-malic acid) [17] and *N*-succinyl chitosan (NSCS) [18].

In particular, *N*-succinyl chitosan (NSCS) is introduced and studied [19]. NSCS is obtained from introduction succinyl groups into amino groups of the glucosamine units of chitosan (Figure 1.2). NSCS has been studied for encapsulating

the various drugs. It was demonstrated that NSCS has great potential performance in drug controlled release delivery because it can be self-assembled and well-dispersed in distilled water, be stable nanospheres in distilled water, has small size range in 50-100 nm, be non-toxicity as well as cell-compatibility. Besides, NSCS easily reacts with the variety of reagents due to the $-NH_2$ and $-COOH$ groups [14-15]. Furthermore, NSCS has been reported to inhibit the proliferation of K562 cells (leukemic cell lines) with the IC_{50} value of 14.26 µM [20].
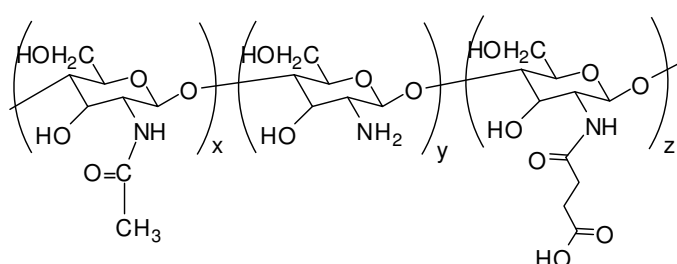
Figure 1.2 Chemical structure of NSCS

In addition, many researchers have been studied NSCS attaching with the active groups or drug molecules to improve bioavailability, prolong action, decrease toxicity, achieve high selectivity of action and solve formulation problems [21]. The examples of active groups are 5-aminosalicylic acid [22], gene [23], mitomycin C [24], lactose [25] and cholesterol [26].

Nowadays, herbal medicines are widely used for treatment many diseases because they exhibit broad spectrum of activities and low side effects. *Androgaphis paniculata* (Burm.f.) Nees (Acanthaceae) is one of the most herbal popular which uses for treatment many diseases and cultivated in China and Thailand. Andrographolide (AG) (Figure 1.3a) is the major bioactive in this plant and display a variety of the pharmacological activities such as anti-inflammatory, anti-viral, anti-platelet aggregation, hepato-protective effects and anticancer activities [27]. Moreover, succinyl group attached at C-14 position of AG (andrographolide-14-α-*O*-succinate, Figure 1.3b) shows higher cytotoxicity toward human leukemic cell lines than AG [28].
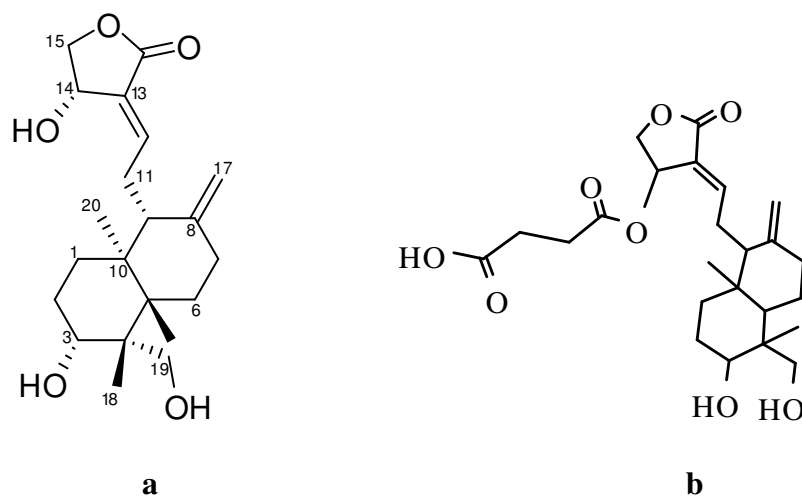
Figure 1.3 Chemical structures of : a) andrographolide and b) andrographolide-14-α-*O*-succinate

Therefore, the purpose of this work is to prepare andrographolide-14-α-*O*-succinate grafting onto chitosan chain which can self-assembly to form nanoparticles. The resulting polymers are characterized by ^{1}H NMR and FTIR techniques. Moreover, the physicochemical and other properties of particles are analyzed by DLS, DSC, XRD, TGA and SEM. Morover, we aims that these particles exhibit biological activities, especially anti-cancer activity, by andrographolide moiety.

1.2 The Objective of Research

To synthesize and characterize chitosan derivative, andrographolidesuccinate grafted chitosan, which possess anticancer activity.

1.3 The Scope of Research

Andrograpolide (AG) is isolated from the whole parts of *Androgaphis paniculata* plants using method previously reported [27]. Then andrographolidesuccinate grafted chitosan (AGS-*g*-CS) is synthesized in 3 steps. First step, 2,2-dimethoxypropane is used as a protecting group for two hydroxyl groups at the C-3 and C-19 positions of AG and then it is reacted with succinic anhydride. A

succinyl moiety is linked at the C-14 position of AG to afford the andrographolide-14-α-*O*-succinate. Finally, andrographolide-14-α-*O*-succinate is grafted onto chitosan backbone. The physicochemical properties of AGS-*g*-CS are analyzed by ^{1}H NMR, FTIR DLS, DSC, XRD, TGA and SEM analysis. The critical aggregation concentration (CAC) is investigated by pyrene fluorescence probe method [29]. Moreover, AGS-*g*-CS is examined for its anti-cancer activity towards cervical cancer (CaSKi cell lines) and breast cancer (MCF-7 cell lines).

CHAPTER II

THEORY AND LITERATURE REVIEWS

In this study, a new chitosan derivative is synthesized by attaching a derivative of andrographolide, andrographolide-14-α-*O*-succinate, to chitosan. The chemical structure of the chitosan derivative is characterized by ^{1}H NMR and FT-IR analysis. In addition, this chitosan derivative colud self-assembly and had anti-cancer activity for using as carrier in drug delivery system. Therefoer, this chapter presented the theory and literature reviews which concerned to this research including drug delivery sytem, drug carrier, chitosan and andrographolide.

2.1 Drug Delivery System

Drug delivery system is used to solve the problems of therapeutic efficiency from administered drugs. Since the major amount of administered drug is metabolized by the body or distributed over the normal tissues and organs that are not involved in the pathological process [1]. Whereas, the only small quantity of administered drug reach to the target sites. In addition, some drugs possess unsuitable properties to use in the human body such as high toxicity, fat solubility, too high or too low water solubility, unstable and many side-effects [30].

Moreover, the concentration of administered drug after taking into the body is also concerned. For intravenous injection drug, the plasma concentration of drug is slowly decreased for overtime. Thus, the dosage and dosage frequency for the patients must be increased, whereas the plasma concentration of orally administered drug and intramuscular injection drug shows the valley peak. If the range of concentration is appropriate, the maximum benefit is derived. On the contrary, the drug concentrations above or below this range can be toxic or ineffective, as exhibited in Figure 2.1 [31].
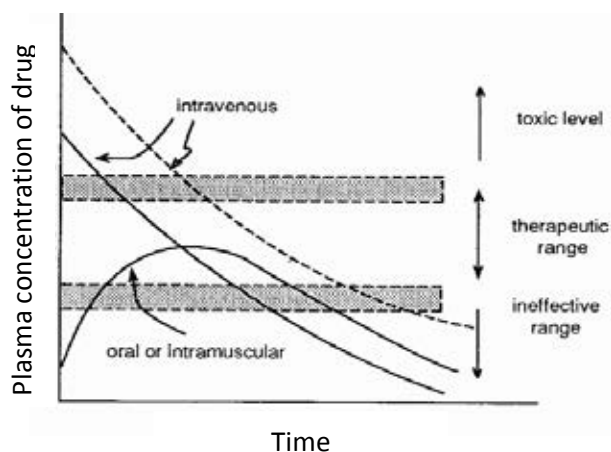
Figure 2.1 Concentration range of conventional dosage form

Therefore, the drug delivery system in the controlled release dosage form was applied to use in the human body. This system can control the rate of drug delivery, the target area of drug administration and maintain therapeutic levels of drug with narrow fluctuations which results in the reduction of toxic or undesirable side effects of drug. The plasma concentration of drug released from controlled release dosage form fluctuates within the therapeutic range over a long period of time (Figure 2.2). That makes it possible to reduce the frequency of drug administration to encourage patients to comply with dosing instructions [32].
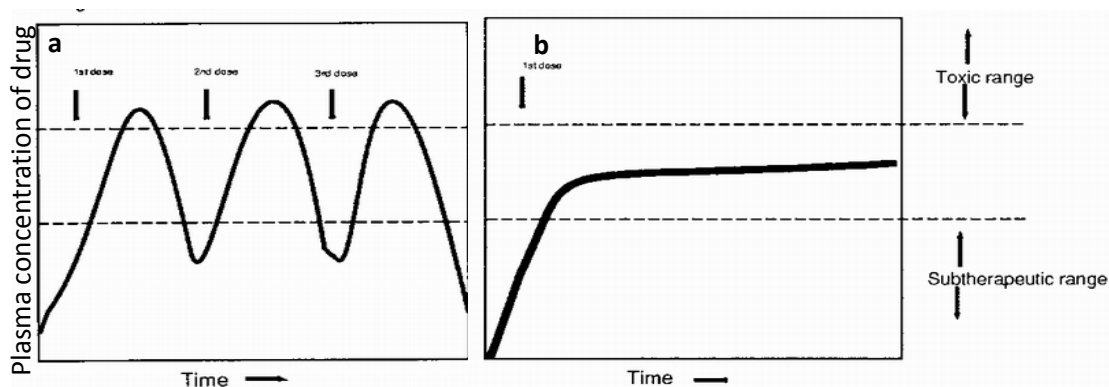
Figure 2.2 The plasma concentration of drug in the patient as a function of time after administration : a) traditional delivery system with repetitive administration and b) prolonged delivery system.

As a result, drug delivery system can improve and control the pharmacokinetics, pharmacodynamics, non-specific toxicity, immunogenicity, biorecognition, efficacy of drug and other problems.

Drug delivery systems are based on interdisciplinary approaches that combine polymer science, pharmaceutics, bioconjugate chemistry, and molecular biology [31]. This system is used for administered the drugs or pharmaceutical compounds into the body and reach the therapeutic area. Drug delivery can be achieved to the target site with various approaches.

Examples of types of drug delivery systems: [31]

1. Membrane diffusion controlled drug delivery system

2. Matrix diffusion controlled drug delivery system

3. Membrane dissolution controlled drug delivery system

4. Osmotic pressure-activated drug delivery system

5. Hydrodynamic pressure-activated drug delivery system

6. Vapor pressure-activated drug delivery system

7. Magnetic force-activated drug delivery system

8. pH-activated drug delivery system

9. Ion-activated drug delivery system

10. Swelling-activated drug delivery system

11. Feedback-regulated drug delivery system

12. Bioerosion-regulated drug delivery system

13. Self-regulating drug delivery system

14. Prolongation of gastrointestinal transit time

15. Intragastric floating tablet

16. Intragastric drug delivery device

17. Gastro-inflatable drug delivery device

18. Bioadhesive stomach, duodenum, transverse colon

19. Targeted or site-specific drug delivery system

All of these systems, the release of drug molecule from the carrier is activated by some physical, chemical, or biochemical processes. In addition, innovative drug-delivery systems are being designed to guide drugs more precisely to tumor cells with the aim of lan ding more of a drug onto the target tissue and less onto normal tissues [7, 33]. The drug delivery of tumor cells can be approached in 2 ways – passive and active processes.

Passive targeting

This process uses the permeability of drug carrier in the vessels at tumor tissue. Due to the tumor tissue cosists of many capillaries, the chemotherapeutic drug is easily served and taken to tumor environment. The permeability of drug carrier is based on 2 factors: (1) the capillary endothelium in malignant tissue is more disorderly as opposed to normal tissue. Thus, the carriers can be permeated to cancer tissue better than normal tissue. (2) The tumor tissue without the lymph node, thus it makes the drug to be eliminated by this gland and accumulate in tissues. Therefore, the concentrations of polymer-drug conjugate (drug carrier) in tumor tissue can reach level 10 to 100 times higher than the administration of free drug [33] (Figure 2.3).
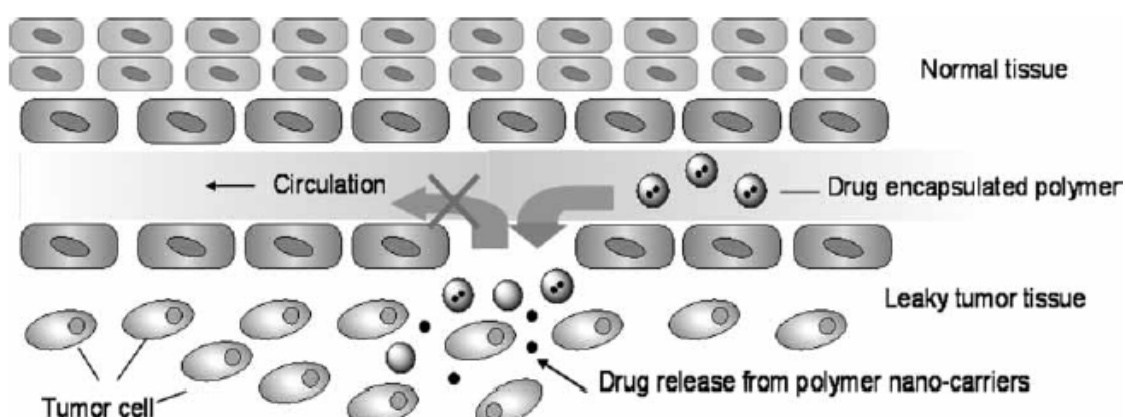
Figure 2.3 Enhanced permeability and retention affect [6]

Active targeting

This process is carried out by attaching the specific ligands of nanoparticles with a targeting moiety of pathological cells (Figure 2.4b). Then the environment of tumor cell (cancer-specific enzymes, high or low pH at the tumor site) makes nanoparticle or pro-drug converting to the active drug. Thus the drug must be designed to select and interact only with the intended target site and minimizing side effects. The pathological cell has many surface targeted such as carbohydrate targeted, receptor targeted and antibody targeted [33, 34].
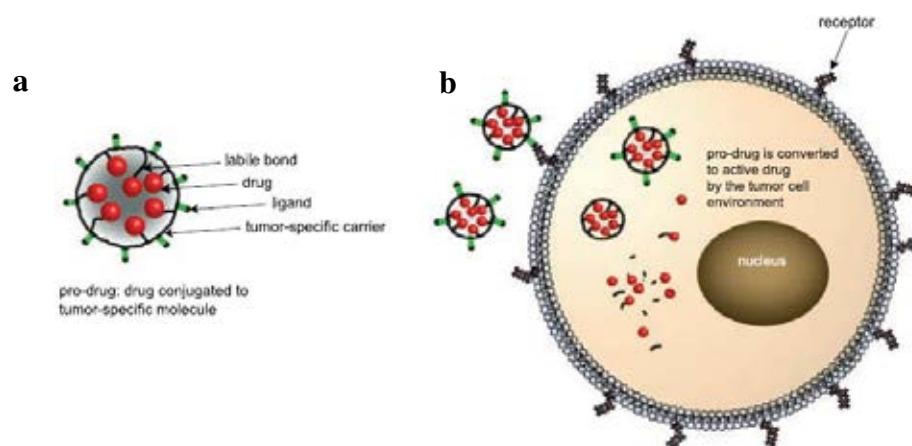
Figure 2.4 a) Pro-drug : drug conjugated to tumor-specific molecule and b) The process of active targeting [33]

2.2 Drug Carrier

Drug delivery systems reside the carrier to contain the drug, which controlled drugs release to the active site. The types of carriers for drug delivery system are, for examples, liposomes, solid lipid nanoparticles, phytosomes, micro/nano emulsion, polymeric micro/nano particles, and dendrimers (Figure 2.5) [35]. Each type shows different pharmacokinetics and pharmacodynamics of drugs [1].
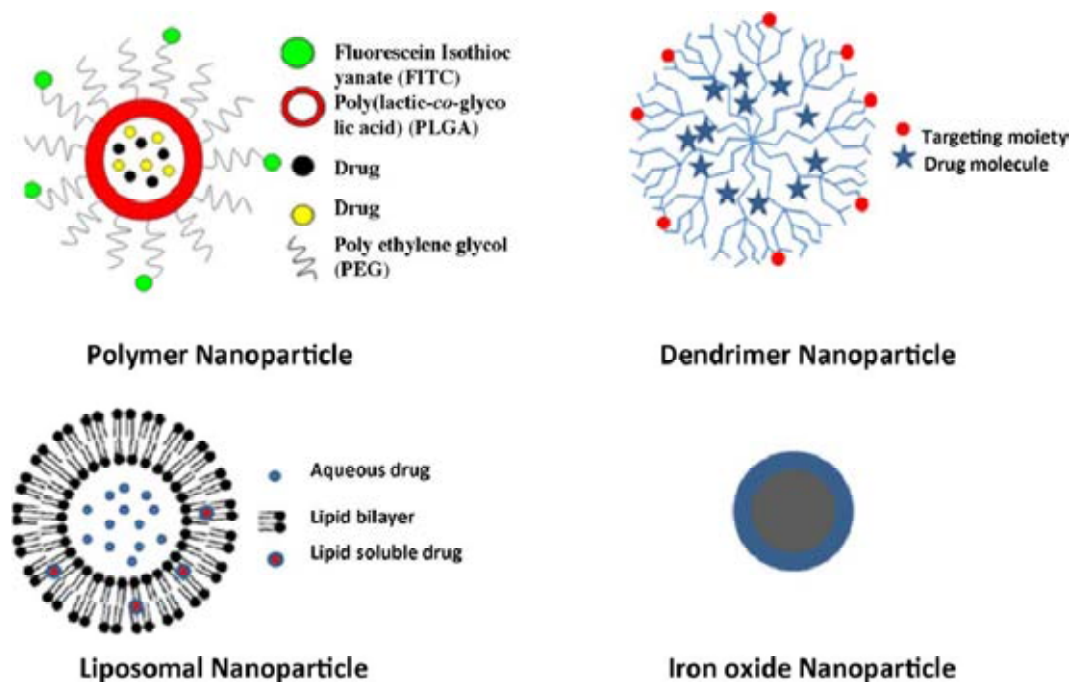
Figure 2.5 Pharmaceutical carriers [35]

The design of carrier has been developed continuously. In order to design the carrier for activation or release at therapeutic area, the difference of required quality and required quantity between the environment of therapeutic area and non-therapeutic area should be considered [30]. However, in nowadays, the nano-sizes of carriers have received increasing attention. Nanocarriers are solid colloidal particles with diameter ranging from 1-1000 nm. Thus, they can pass through the smallest capillary vessels and avoid rapid removal by phagocytes resulting in their prolonged duration in blood stream. They can penetrate through cells and tissue gaps to achieve target organs. Moreover, the outstanding advantages of this system are showing controlled release properties, improving the utility of drugs and reducing toxic side effect [6].

Nanoparticles are mainly divided into 2 types which depending on preparation process: nanocapsules and nanospheres (Figure 2.6) [36]. Nanosphere is a matrix which the drugs are dispersed or adsorbed throughout the matrix whereas nanocapsule is a membrane wall which the drugs are entrapped or surrounded in membrane.
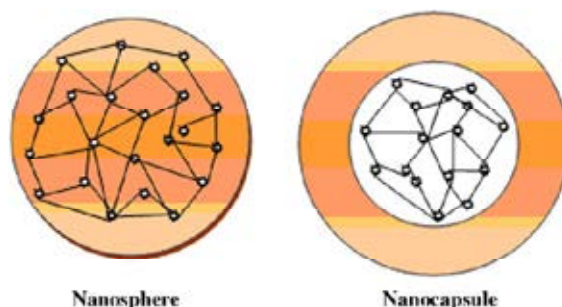
Figure 2.6 Schematic representations of nanoparticles [36]

Recently, many researchers have been studied about polymeric materials used as nanoparticles. Polymer was used in drug delivery system since 1960 [4]. Polymeric materials in drug delivery must be safe, biocompatible, biodegradable in human body and not cause excessive immune responses [8]. It can be both synthetic and natural polymers. There are many types of polymeric materials and one of those is a polymer-drug conjugate model. This type was firstly investigate by Ringdorf in 1975 and it could improved the chemical and physical properties of native polymer [37]. The aim of this technology is to diagnose and to treat disease. This technology is integrated the medicine and nanotechnology.

Polymer-drug conjugate versus drug encapsulate

The purpose of both polymer-drug conjugate and drug encapsulate is to improve the efficiency of therapeutic drug. The difference of encapsulated drug in polymer carriers and conjugated drug with polymer is the release form of the drug, the drug can be released from polymer carriers (physical encapsulation) by the diffusion method whereas polymer-drug conjugate releases by the cleavage of linkage between the drug and polymers. The polymer-drug conjugate has been developed since 1975. The drug molecules are attached with polymer through covalent or cleavable bond which is generally size around 10 nm or less whereas the physical encapsulation is based on the aggregation of hydrophobic polymer

(polymeric nanoparticles) or the self-assembly of the hydrophobic polymer domain of an amphiphilic block-copolymers (polymeric micelles and vesicles) thus it has the size in a range of 20-100 nm (for micelles) and around 100 nm (for polymer vesicles) (Figure 2.7) [6].
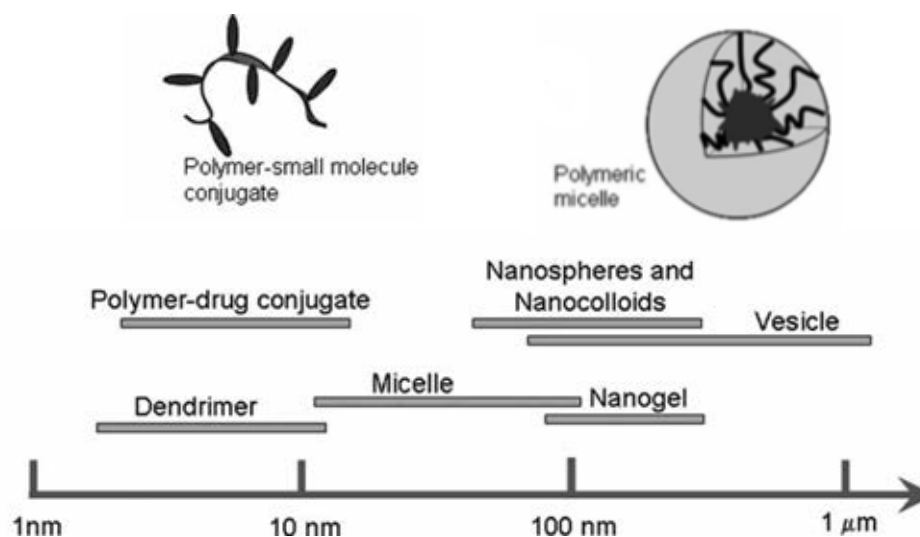
Figure 2.7 The various sizes of polymeric nanomedicine drug delivery systems [6]

In order to release the drug from carrier either polymer encapsulation or polymer-drug conjugate, there are three basic opproaches to release the drug.

(1) The erosion of polymer surface: this process resides the environment of the therapeutic area, which has effect on the destruction of physically entrapped drug.

(2) The cleavage of covalent bond of polymer and drug: the drug is cleaved from the polymer carrier and release by diffusion.

(3) The diffusion of the drug from polymer carrier: the controlled release of diffusion depends on the bioabsorption of polymer, and it delayed until after drug depletion.

All three processes can evade any irreproducibility of the bioerosion rate and the difficulty of trying to synchronize the diffusion and bioerosion processed to achieve a specified delivery rate (Figure 2.8) [38].
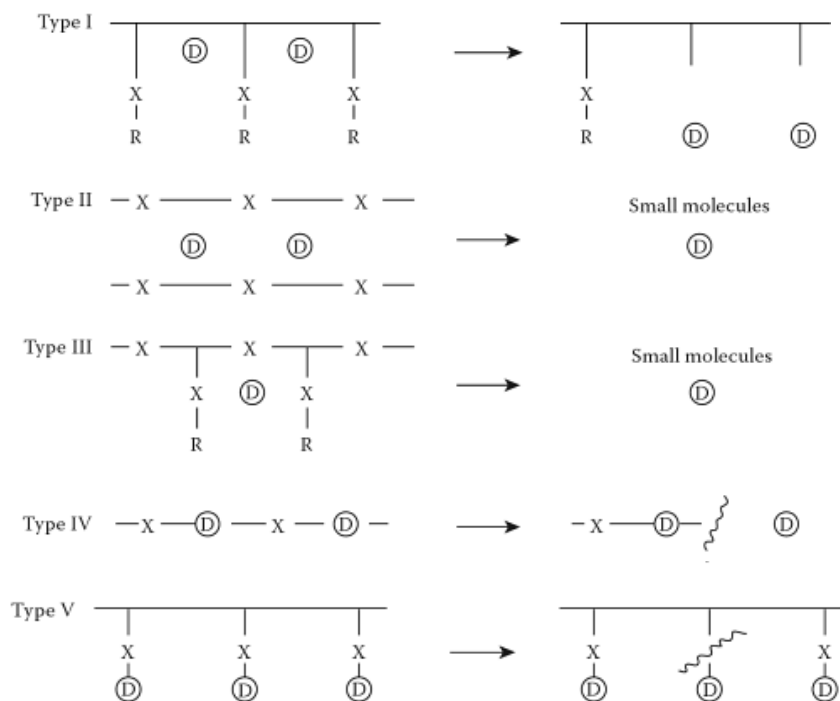
Figure 2.8 Different approaches to drug delivery systems based on biodegradable polymer, X : a bio-labile linkage; D : a drug molecule [38]

2.3 Chitosan

A lot of the marine waste (crab shell, shrimp shell and squid pen) from manufacturing industries has been sold at very low price for animal feed. Thus, in order to increase the price of these wastes, the chemical properties of marine wastes have been applied to use.

Chitosan, a biodegradable carbohydrate, is produced from marine wastes. It is obtained from alkaline deacetylation of chitin, which is a linear polymer of *N*-acetyl-2-amino-2-deoxy-deglucopyranose units linking with β-(1-4) bonds. Chitin present in the outer structure of crustaceans, insects and a component of the cell walls of bacteria or fungi [39]. When the degree of deacetylation of chitin has more than 50%,

it is called "chitosan" (Figure 2.9) and soluble in aqueous acidic media (pH < 6.5) [10]. However, chitosan is insoluble in water and organic solvent.
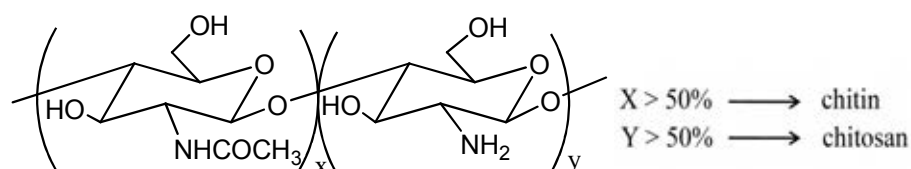
Figure 2.9 Chemical structures of chitin and chitosan.

Chitosan is widely used in many fields such as food, agricultural, industrial, cosmetic especially pharmaceutical and medical because it has a lot of good properties including nontoxicity, biocompatibility, mucoadhesivity, and biodegradability [40]. Chitosan contains three reactive functional groups per a glucosamine unit including 1) secondary hydroxyl group at C-3 position, 2) primary hydroxyl group at C-6 position and 3) amino group at C-2 position [13]. These functional groups in chitosan structures allow various chemical modifications of chitosan such as *N*-carbonylation, acylation, alkylation, *N*-carboxyalkylation, *N*-acylation, *O*- and *N*-succinylation and shift base formation [41]. Although chitosan would be expected to attract even more numerous applications. However, chitosan has limited solubility in water because of its strong intermolecular hydrogen bonding (H-bond) [10]. Therefore, many researches have been reported to solve the strong intermolecular hydrogen bonding of chitosan by modifying chitosan structure.

N-Succinyl chitosan (NSCS), a chitosan derivative, is obtained from introduction succinyl groups into amino groups of the glucosamine units of chitosan (Figure 2.10a). Succinyl moiety can be easily attached on chitosan chain and succinylation degree substitution can be optimized by changing the reaction conditions [42]. NSCS with the succinylation degree more than 65% can be dissolved in alkaline but not in acidic, opposite to the native chitosan [43]. NSCS is initially developed as a wound dressing material [44] and a vesicle for various drugs. It has

great potential performance in drug controlled release delivery because it is non-toxic, cell compatibility, and well-dispersion in distilled water [12]. Moreover, it can self assembly to form stable nanospheres in distilled water with a small size range in 50-100 nm (Figure 2.10b). This nanosphere does not require the high temperature, organic solvent, surfactant and some other special experimental technology for forming the particle [12]. The physical properties of NSCS (degree of substitution, solubility, isoelectric point, glass transition temperature, partition coefficient and zeta potential) are confirmed for basic or applied purpose in biomedical and pharmaceutical science stabilization [11]. Furthermore, NSCS nanoparticles can be inhibited the proliferation of leukemic cell lines with the IC_{50} value of 14.26 μM (24h), which is carried out by necrosis and apoptosis induction in this leukemic cells [20]. The plasma half-lives of NSCS in normal mice and Sarcoma 180-bearing mice are found to be 100.3 h and 43 h, respectively, which longer than those of other long-circulating macromolecules reported to date [45].
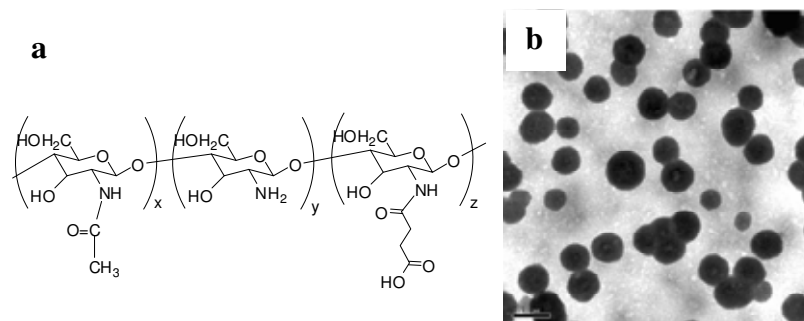
Figure 2.10 a) Chemical structure of NSCS and b) TEM image of NSCS nanoparticles [12]

In addition, NSCS easily reacts with the variety of reagents due to the $-NH_2$ and $-COOH$ groups [12]. Thus, many researchers have been studied NSCS attaching with the active groups or drug molecules for using in drug delivery systems to improve bioavailability, prolong action, decrease toxicity, achieve high selectivity of action and solve formulation problems [21]. For examples,

Kato *et al.* [24] prepared NSCS conjugating with mitomycin C (MMC) which was an anti-cancer agent. This conjugate showed antitumor activities towards various tumors which was better than MMC.

Kato *et al.* [25] prepared lactose grafting on NSCS (Figure 2.11), which used as a liver-specific drug carrier. Lactosaminated *N*-succinyl chitosan was injected intravenously with high and low doses. The result showed maximum liver localization at 8 h for both doses. The liver distribution of lactosaminated *N*-succinyl chitosan might be involve with asialoglycoprotein receptor.
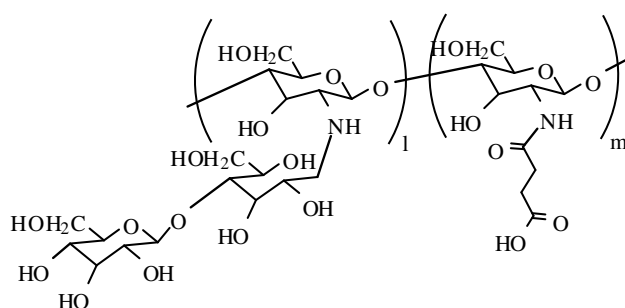
Figure 2.11 Chemical structure of lactosaminated *N*-succinyl chitosan [25]

Wang *et al.* [26] prepared NSCS grafting with cholesterol (CHCS). The degree of cholesterol substitution on chitosan was found to be 7.3 % by ^{1}H NMR analysis and the critical aggregation concentration was 1.16×10^{-2} mg/mL (in 0.1 M acetic acid). CHCS could be self-assembled with spherical shape with the mean diameter of 417.2 nm in aqueous media.

18
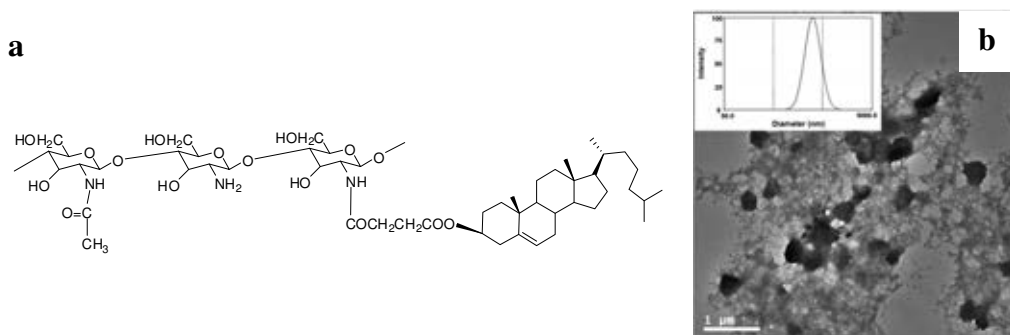
Figure 2.12 a) Chemical structure of CHCS and b) TEM image and size distribution of CHCS nanoparticle [26]

2.4 Andrographolide

Androgaphis paniculata (Burm.f.) Nees (Acanthaceae), a herbal plant used traditionally to treat various diseases [46], is mostly cultivated in Thailand, China and India. The major compound of this plant is andrographolide (AG) which has the chemical structure as illustrated in Figure 2.13a. It is a bicyclic diterpenoid lactone which contains three hydroxyl groups at C-3, C-19 and C-14 positions [47]. It has been reported to exhibit a wide spectrum of pharmacological properties such as anti-inflammatory, anti-viral, anti-platelet aggregation, anti-cancer activities, immunomodulation, anti-infection, anti-hepatotoxicity, anti-atherosclerosis, anti-hyperglycemice effect, anti-oxidation, anthelmintic activity, analgesic and anti-pyretic effects [27, 46, 48]. The appearance of AG is colorless crystal with bitter taste.
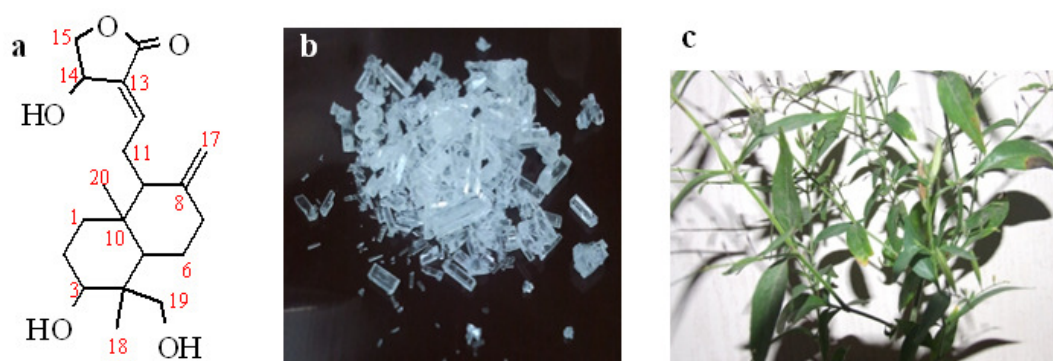
Figure 2.13 a) Chemical structure of AG, b) The crystals of AG and c) *A. paniculata* Nees plants

However, AG dissolve slightly in ether and water whereas it easily dissolved in MeOH, EtOH, pyridine, acitic acid [49]. The low solubility in water of AG is limited for using in pharmaceutical field because the solubility is one of important factors to achieve desired concentration of drug in systemic circulation for achieving required pharmacological response. Thus, the poorly water soluble drugs must be required high dosage in order to reach the therapeutic plasma concentrations after administration [50]. Therefore, many researches have been reported to solve these problems by increasing the solubility of AG. For examples,

In 2000, Onlaor *et al* [51] prepared the microcapsules for encapsulating the *A. paniculata* extract by using Eudragit RL 100 as a wall polymer. This microcapsules were prepared via oil in oil solvent evaporation technique. The ratio of polymer and the *A. paniculata* extract was studied. The 1:1 core to wall ratio showed the highest yield and drug content, whereas the 1:2 ratio gave the highest core entrapment.

a

1:1 core to wall ratio

1:2 core to wall ratio

b
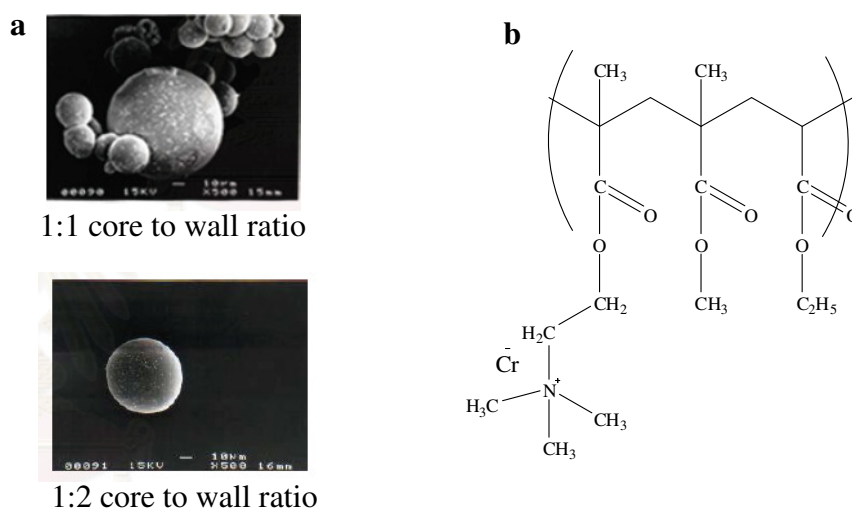
Figure 2.14 a) The SEM image of microcapsules of *A. paniculata* extract and b) Chemical structure of Eudragit RL 100 [51]

In 2002, Zhao *et al.* [52] prepared an inclusion complex of β-cyclodextrin and AG by using a convenient new method of microwave irradiation. The results from ^{1}H NMR and two dimensional NOE spectroscopic measurements were indicated that the stoichiometry of complex formation was found to be 1:1 (guest:host ratio) and the two isomeric 1:1 inclusion complexes were concurrently presented in the solution.
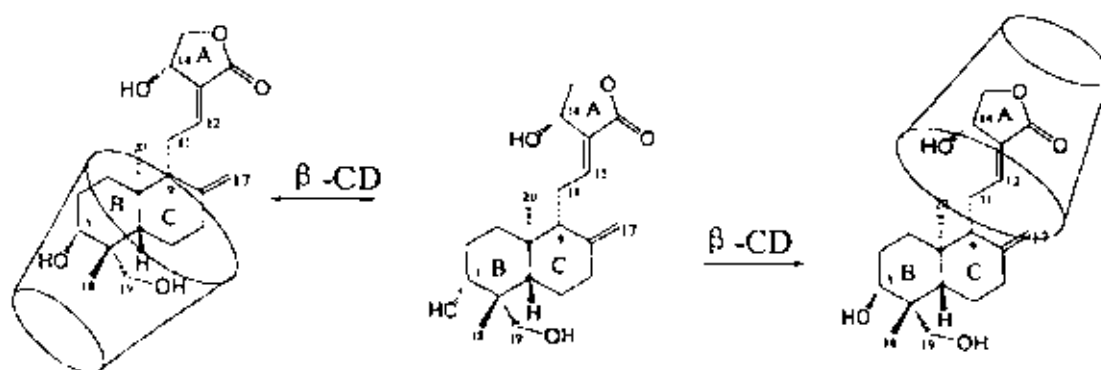
Figure 2.15 The model of AG / β-cyclodextrin inclusion complex [52]

In this study, we are interesting in improve water solubility and anti-cancer activity of AG. AG has been reported to inhibit many cell lines which were summarized in Tables 2.1.

Table 2.1 Anticancer activities of andrographolide

Cancer type	Cell line	GI$_{50}$ (µg/mL)	IC$_{50}$(µg/mL)	Reference
Colon	HT-29	10	-	[53]
Leukemia	HL-60	9.33	-	[54]
	U 937		4.50	[28]
	THP1	-	2.34	[28]
	K562	-	14.65	[28]
Breast	MCI/ADR-RES	15	-	[53]
Central nervous system (CNS)	U251	10	-	[53]
Colon	SW620	11	-	[53]
Lung	H522	16	-	[53]
Melanoma	M14	11	-	[53]

Cancer type	Cell line	GI$_{50}$ (µg/mL)	IC$_{50}$(µg/mL)	Reference
Ovarian	SKOV3	18	-	[53]
Prostate	DU145	12	-	[53]
Renal	A498	28	-	[53]
Colorectal (Colon & Rectal)	Lovo	8.6	-	[55]
Hepatocellular	SMMC-7721	-	200	[56]

*GI$_{50}$ is the concentration of drug to cause 50% reduction in proliferation of cancer cells i.e. growth and IC$_{50}$ is the maximal concentration of drug to cause 50% inhibition of biological activity of cancer cells

Moreover, the derivatives of AG have been widely studied and evaluated their bioactivities compared with AG. Andrographolide-14-α-*O*-succinate (Figure 2.16) is synthesized and evaluated anticancer activity. Andrographolide-14-α-*O*-succinate is produced from succinyl moiety attaching at C-14 position of AG, which shows higher cytotoxicity toward human leukemic cell lines than AG (Table 2.2) [28].
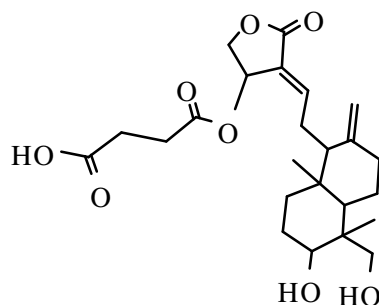
Figure 2.16 Chemical structure of andrographolide-14-α-*O*-succinate

Table 2.2 Anticancer activit**ies** of andrographolide (AG) and andrographolide-14-α-
O-succinate

Compound	IC50 (µM)				
	Leukemic cell line			Normal cell line	
	U937	THP1	K562	L132	NIH3T3
AG	12.87	6.69	41.85	53.8	44.5
Andrographolide-14-α-*O*-succinate	5.47	5.84	25.30	8.50	44.5

Therefore, the purpose of this work was to prepare andrographolide-14-α-*O*-
succinate grafting onto chitosan chain in order to create the self-assembly of
nanoparticles used as drug delivery system. Furthermore, the andrographolide-14-α-*O*-
succinate grafting onto chitosan chain may also synergy with the drugs. Thus the
efficiency of therapy was improved which not only acts as deliverer but also active
specie.

CHAPTER III

EXPERIMENTAL

3.1 Chemicals and Materials

- The dried whole plant of *Androgaphis paniculata* was purchased from Thai herbal pharmacy (Chao Krom Pler Dispensary)
- Andrographolide, 98%, for R&D use only (Sigma-Aldrich, Germany)
- Chitosan $\overline{M}_w$ of 25 kDa and a degree of deacetylation (DD) of 90% (Taming Enterprises Co., Ltd, Thailand)
- 2,2 dimethoxypropane (Sigma-Aldrich, Germany)
- Succinic anhydride (Acros oraganics, Geel, Belgium)
- Pyridinum *p*-toluenesulphonate (ppts) (Sigma-Aldrich, USA)
- Dimethylaminopyridine (DMAP) (Acros oraganics, Geel, Belgium)
- Benzene, analytical grade (Carlo erba reagents)
- Dimethyl sulfoxide (DMSO), analytical grade (Labscan, Dulin, Ireland)
- Dichloromethane (CH_2Cl_2), analytical grade (Merck, Germany)
- *N,N*-Dimethyl formamide (DMF), analytical grade (Labscan, Dulin, Ireland)
- *N*-hydroxy-succinimide (NHS) (Sigma-Aldrich, Germany)
- 1-Ethyl-3(3-dimethylaminopropyl) carbodiimide (EDC) (Acros organics, Geel, Belgium)
- Hydrochloric acid (HCl) (Carlo Erba Reactifs SA)
- Hexane (Carlo Erba Reactifs SA)
- Ethyl acetate (EtOAc) (Carlo Erba Reactifs SA)
- Triethylamine, analytical grade (Carlo erba reagents)
- Sodium sulphate anhydrous (Na_2SO_4) (Carlo Erba Reactifs SA)
- Silica gel 60 No. 7734 (Merck)
- Silica gel 60 PF 254 precoated aluminium sheets (Merck Kieselgel)
- Anisaldehyhide dripping reagent was obtained from the mixture solution of MeOH : anisaldehyde : conc.H_2SO_4 (95:3:3 (v/v) ratio).

- Universal indicator (pH-indicator strips) (Merck, Germany)

- Cellulose dialysis membranes $\overline{M}_w$ cut off at 11,011 Da (Sigma-Aldrich, Germany)

- 0.2 µm Nilon filter (Vertical Chromatography Co, Ltd)

- Methanol (MeOH), HPLC grade (Merck, Germany)

- Milli Q water

- HPLC column, ACE 5 C18-AR column (150 mm × 4.6 mm)

- Pyrene (Acros oraganics, Geel, Belgium)

3.2 Instruments

Table 3.1 Instruments

Instruments	Manufacture	Model
High performance liquid chromatography	Waters Alliance	600
Evaporator	Buchi	R114
Fluorescence spectrometer	Varian	Cary Eclires
Particle sizer	Malvern Instruments	Zatasizer Nanoseries
Fourier transform infrared spectrometer	Nicolet	6700
Freeze dryer	Labconco	FreeZone 77520
Differential scanning calorimeter	NETZSCH	DSC 204 F1
X-ray diffractometer	Phillips	PW 3710 BASED
Scanning electron microscope	Phillips	XL30CP
Nuclear magnetic resonance spectrometer	Varian	Mercury plus 400 MHz

3.3 Method

PART I: Extraction of Andrographolide from *A. paniculata*

The dried whole plant (2 kg) of *A. paniculata* was extracted with 5 L methanol (MeOH) for 2 days, and the residue was re-extracted with 5 L methanol for 5 times. The combine methanolic extract was concentrated using a rotary vacuum evaporator, yielding after evaporation was 250 g. The crude extract was re-dissolved in methanol and de-colored by charcoal. After filtration, the concentrated residue was subjected to a vacuum column chromatography (VCC) with a gradient eluent of methanol in dichloromethane (0–20%). Five combined fractions were obtained (Fractions A–E). Fraction B was re-crystallized using MeOH to give AG (8.356 g). Finally, the chemical structure of the isolated AG was elucidated by spectroscopic data (^{1}H NMR and ^{13}C NMR) and comparing with those of standard AG (andrographolide, 98%, Sigma-Aldrich Co., Ltd.). Moreover, the purity of the isolated AG was determined by HPLC method using a reverse-phase ACE 5 C18-AR (150 mm × 4.6 mm) column and MeOH : H$_2$O (60 : 40) solvent system.

PART II: Synthesis and Characterization of Andrographolidesuccinate grafted chitosan (AGS-*g*-CS)
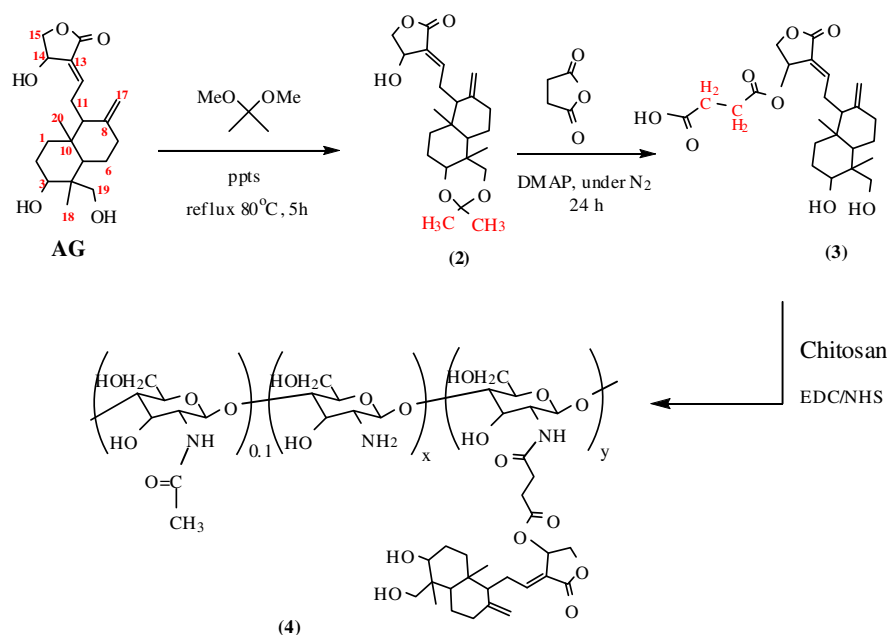
Scheme 3.1 Overall process andrographolidesuccinate grafted chitosan of synthesis

Scheme 3.1 shows the overall synthesis scheme of andrographolidesuccinate grafted chitosan, which was divided into 3 steps. Firstly, the 2,2-dimethxypropane was used as a protecting group for two hydroxyl groups at the C-3 and C-19 positions of AG to obtain 3,19-isopropylidene-andrographolide (**2**). Then **2** reacted with succinic anhydride with dimethylaminopyridine (DMAP) in N_2 atmosphere. A succinyl moiety was linked at the C-14 position of AG to afford andrographolide-14α-*O*-succinate (**3**). Lastly, **3** was further grafted onto chitosan backbone to obtain andrographolidesuccinate grafted chitosan (AGS-*g*-CS, **4**).

3.3.1 Synthesis of 3,19-Isopropylidene-andrographolide (2)
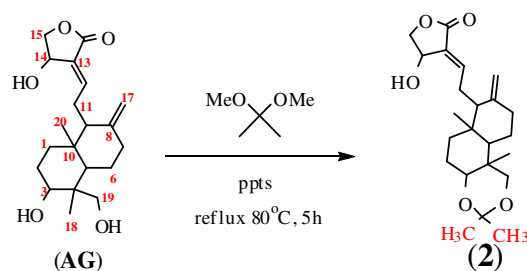
Scheme 3.2 Synthesis of 3,19-isopropylidene-andrographolide

The hydroxyl groups at C-3 and C19 positttions of AG were protected accroding to method of S.R. Jada [47]. Briefly, a mixture of AG (1.05 g, 3 mmol) and 2,2 dimethoxypropane (1.5 ml, 12 mmol) in 30 mL of a solvent mixture (benzene and DMSO = 7.5:1) with a catalytic amount of pyridinum *p*-toluenesulphonate was heated to reflux 80 °C for 5 h. Subsequently the mixture was cooled to room temperature, then basified by triethylamine until universal paper changing to green color, diluted with benzene and washed with distilled water for three times. The organic layer was dried with anhydrous Na_2SO_4 and concentrated to obtain 3,19-isopropylidene-andrographolide (**2**, 0.92 g, 2.34 mmol, 78%) as a white solid precipitate.

3.3.2 Synthesis of Andrographolide-14-α-*O*-succinate (3)
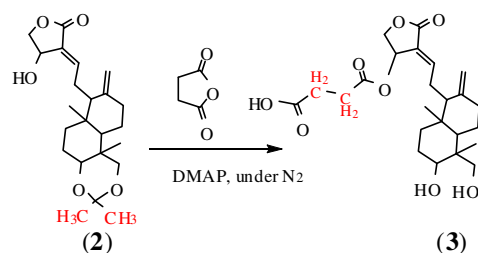
Scheme 3.3 Synthesis of andrographolide-14-α-*O*-succinate

Succinic anhydride (92.4 mg, 0.92 mmol) and DMAP (6.0 mg, 0.05 mmol) were added to a solution of **2** (0.3 g, 0.77 mmol) in 12 mL of dry dichloromethane. This mixture was stirred under a nitrogen atmosphere at room temperature for overnight. The solvent was removed under reduced pressure and the residue was purified by a silica gel column chromatography using a gradient system of hexane and ethyl acetate as eluent to afford andrographolide-14-α-*O*-succinate (**3**, 0.17 g, 0.4 mmol, 49%).

3.3.3 Synthesis of Andrographolidesuccinate grafted chitosan (AGS-*g*-CS, 4)
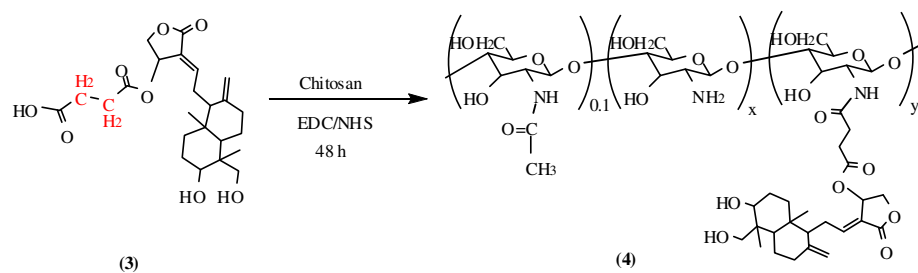
Scheme 3.4 Synthesis of andrographolidesuccinate grafted chitosan

N-hydroxy-succinimide (93 mg, 0.81 mmol) and 1-ethyl-3-(3-dimethyl aminopropyl) carbodiimide (125 mg, 0.81 mmol) were added into a solution of chitosan (130 mg, 0.81 mmol) in 13 mL of 0.1 % hydrochloric acid. Subsequently, a solution of **3** (365 mg, 0.81 mmol) in 73 mL of dimethylfomamide (DMF) was slowly dropwised into this mixture and stirred at room temperature for 48 h. The whole solution was dialyzed with a dialysis membrane (molecular weight cut-off = 11,011)

against distilled water for 3 days to remove excess DMF and other reagents. The product solution was turned to be a milky solution which indicates that it might be form self-assembly. Thus, this colloidal solution was further determined its morphology, particles size and zeta potential. A part of product solution was further freeze-dried to obtain andrographolidesuccinate grafted chitosan (AGS-*g*-CS, **4**) powders and stores in desiccator until used for ^{1}H NMR and FTIR analysis.

3.3.4 Characterization of Andrographolidesuccinate grafted chitosan (AGS-*g*-CS)

3.3.4.1 Nuclear Magnetic Resonance spectroscopy (NMR)

The chemical structures of AG, 3,19-isopropylidene-andrographolide (**2**), andrographolide-14-α-*O*-succinate (**3**) and AGS-*g*-CS (**4**) were identified by NMR analysis performing on Varian Mercury 400 NMR spectrometer at ambient temperature and all samples were recorded in CD$_3$OD, CDCl$_3$ and D$_2$O solvent systems for AG, **2**, **3** and **4**, respectively.

3.3.4.2 Fourier-Transform Infrared Spectroscopy (FTIR)

The IR spectra were recorded in the wavelength region 4000–400 cm^{-1} on ATR mode using a Nicolet 6700 and Omnic software was used to control the measurement.

3.3.4.3 Differential Scanning Calorimetry Analysis (DSC)

The thermal properties of chitosan, AG and AGS-*g*-CS were investigated by DSC (NETZSCH DSC 204 F1). All samples were put into aluminium vessels and heated from room temperature to 340 °C at a heating rate of 10 °C/min under nitrogen atmosphere.

3.3.4.4 X-ray Diffractometry Analysis (XRD)

The X-ray diffraction patterns of chitosan and AGS-*g*-CS were obtained using Philips PW 3710 BASED diffractometer system with Cu (λ = 1.5406 Å), in the range of 5° « 2θ » 40° (voltage 40 kV, 30 mA).

3.3.4.5 Thermal Gravimetric Analysis (TGA)

Thermal gravimetric analysis was performed with 3-5 mg of chitosan and AGS-*g*-CS in Al_2O_3 crucible under a dynamic nitrogen atmosphere flowing at 50 ml min^{-1}. The samples were run at a scanning rate of 25 °C/min using Pyris 1 Thermogravimetric analyzer (Perkin Elmer, USA).

3.3.4.6 Dynamic Light Scattering (DLS)

The mean hydrodynamic diameter, size distribution and zeta potential of AGS-*g*-CS nanoparticles were measured in distilled water at 25 °C on a Malvern 3000HSA Zetasizer (UK) based on the dynamic light scattering (DLS) techniques.

3.3.4.7 Scanning Electron Microscopy (SEM)

The shape and surface morphology of the particles were examined by scanning electron micrograph (SEM). The product solution from dialysis was diluted with distilled water and ultrasonic treatment for 10 min. The sample was placed on a double-side sticking tape, air-dried and gold spray-coated before examined under transmission electron microscope (Phillips, XL30CP).

3.3.5 Critical Aggregation Concentration (CAC) of AGS-*g*-CS nanoparticles

The critical aggregation concentration (CAC) was estimated to prove the potential of particle formation of AGS-*g*-CS in the distilled water by fluorescence spectroscopy using pyrene fluorescence probe method [57]. Briefly, 3 µL of pyrene solution (1 mM) in MeOH was added into the 10-mL test tube and the solvent was

removed by purging nitrogen gas for 3 min. Then, 3 mL of each concentrations of AGS-*g*-CS in water (0.001, 0.005, 0.01, 0.05, 0.1, 0.15, 0.2, 0.25, 0.35, 0.45, 0.7, 0.8 and 1 mg/ml) were added into the test tube. Thus, the concentration of pyrene in each test tube was 6 µM. The solutions were sonicated for 20 min and kept overnight at room temperature. Then the solution was sonicated for 20 min again before being subjected to spectrofluorometric analysis (λ_{excite} = 334 nm). The fluorescence spectra were recorded with Cary Eclipes spectrofluorometer with the emission wavelength from 300-500 nm. The peak height intensity ratio (I_3/I_1) of third peaks (I_3 at 382 nm) to the first peak (I_1 at 372 nm) against the logarithm of AG-*g*-NSCS concentrations were plotted.

3.3.6 Cytotoxicity Study (MTT assay)

The cytotoxicity of AG, andrographolide-14-α-*O*-succinate and AGS-*g*-CS were determined by colorimetric method, the 3-(4,5-dimethyl-2-thiazolyl)-2,5-diphenyl-2*H*-tetrazolium bromide (MTT) assay [58]. CaSKi cells (cervical cancer) and MCF-7 cells (breast cancer) were seeded in each well of 96-well plates with a density of 5×10^3 cells/well and incubated for 24 h at 37 °C in humidified atmosphere containing 5% CO_2. The cells were fed with the different concentrations of samples (1-5 mg/mL) and treated for 72 h. Then, 10 µL of MTT solution (5 mg/mL in PBS) was added to each well and incubated for 4 h. The medium was carefully removed and DMSO (100 µL/well) was added to dissolve the produced formazan crystal and the absorbance was measured at 540 nm using a microplate reader. Cells treated with only DMSO were used as positive control. The cell viability was shown the results as a percentage of the control by following equation:

$$Viability\ (\%) = \frac{A_t}{A_c} \times 100$$

Where A_t was the absorbance of the cells treated with sample and A_c was the absorbance of the cells untreated with sample.

In order to calculate the IC_{50} values, the sample concentrations were plotted versus the percentage of growth inhibition. The linear equation was used to calculate the IC_{50} followed as;

$$Y = aX + b$$

$$IC_{50} = \frac{(50 - b)}{a}$$

Where a was constant number, b was Y-intercept, X was sample concentration and Y was % inhibition.

CHAPTER IV

RESULTS AND DISCUSSION

This research study was divided into two parts. The first part presented the extraction of andrographolide (AG) from the whole parts of *Andrographis paniculata* and the second part reported the synthesis and characterization of andrographolidesuccinate grafted chitosan (AGS-*g*-CS).

PART I: Extraction of Andrographolide from *A. paniculata*

Androgaphis paniculata or Fa-Tha-lai-Joan is a herbal plant used traditionally to treat various diseases in Thailand, China and India [46]. The major compound of this plant is andrographolide (AG) which has a wide spectrum of pharmacological activities, especially anti-cancer activity. Therefore, AG is selected to use in this study.

AG was isolated as descibed in Part I of Chapter III and characterized chemical structure by ^{1}H and ^{13}C-NMR spectroscopy including comparing with those of the standard AG. The results in Figures 4.1-4.2 and Table 4.1 indicated that the isolated procedure was successful to obtain AG which its chemical structure was shown in Figure 4.3.

Moreover, the purity of the isolated AG was evaluated by HPLC technique. The isolated AG had the retention time (R_t) at 4.604 min with 99.84 % purity (Figure 4.4).
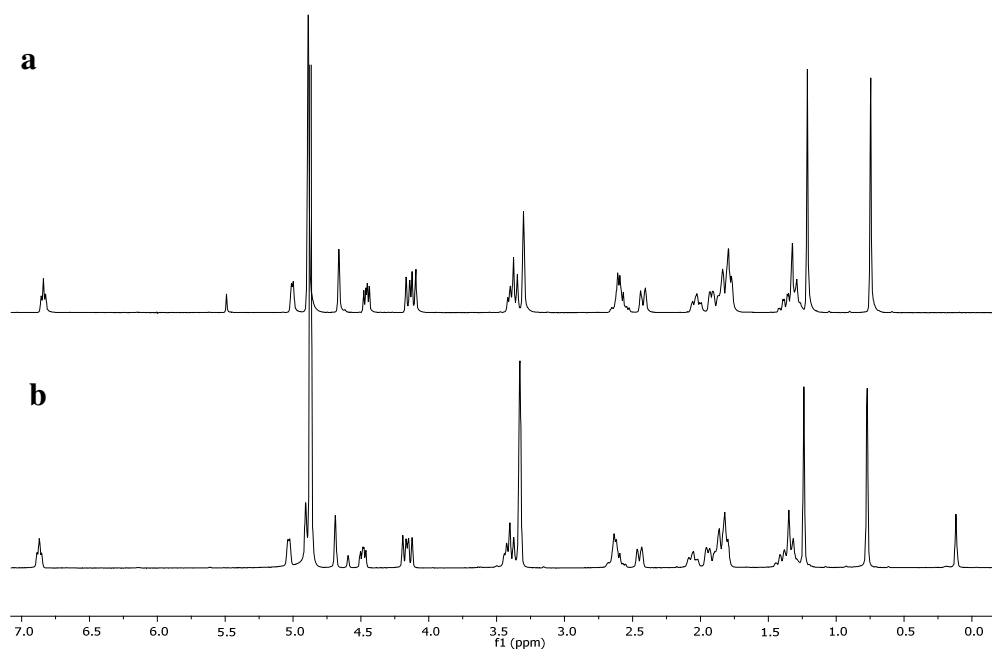
Figure 4.1 ^{1}H-NMR spectrum of: a) the isolated AG and b) standard AG
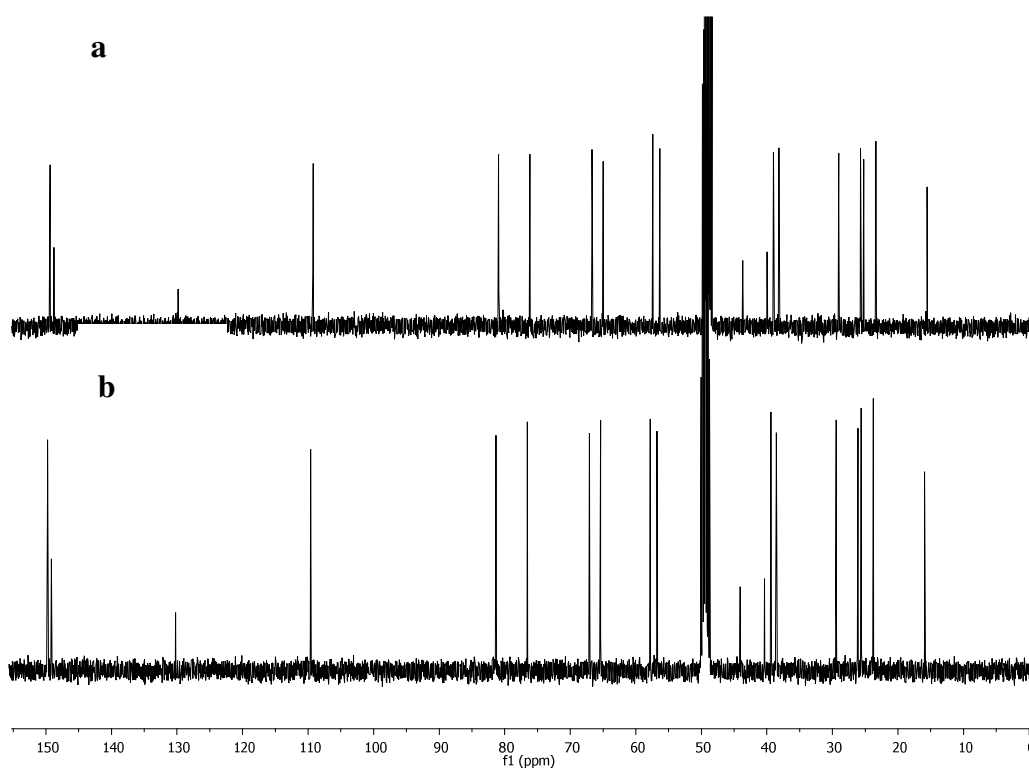
Figure 4.2 ^{13}C-NMR spectrum of: a) the isolated AG and b) standard AG

Table 4.1 The ^{1}H and ^{13}C-NMR chemical shift assignments of the isolated AG compared with those of andrographolide

Position	Isolated AG (CD$_3$OD)		Standard AG (CD$_3$OD)	
	δ_C	δ_H (int., mult., *J* in Hz)	δ_C	δ_H (int., mult., *J* in Hz)
1a	38.15	1.80(1H, s)	38.17	1.84 (1H, s)
1b	38.15	1.26 (1H, s)	38.17	1.29 (1H, s)
2a	29.05	1.76 (1H, s)	29.06	1.80 (1H, s)
2b	29.05	1.74 (1H, s)	29.06	1.78 (1H, s)
3	80.94	3.34 (1H, m)	80.88	3.38 (1H, m)
4	43.70	-	43.78	
5	56.34	1.29 (1H, s)	56.37	1.32 (1H, s)
6a	25.23	1.84 (1H, m)	25.23	1.87 (1H, m)
6b	25.23	1.35 (1H, m)	25.23	1.36 (1H, m)
7a	38.99	2.40 (1H, d, 13.2)	38.99	2.41 (1H, d, 13.6)
7b	38.99	1.99 (1H, m)	38.99	2.00 (1H, m)
8	148.89	-	148.98	
9	57.42	1.89 (1H, dd, 10.4, 2.2)	57.44	1.91 (1H, d, 9.6)
10	40.01	-	39.96	
11	25.73	2.58 (2H, m)	25.74	2.6 (2H, m)
12	149.37	6.80 (1H, t, 6.2)	149.36	6.85 (1H, t, 6.4)
13	129.78	-	129.87	
14	66.67	4.96 (1H, d, 5.6)	66.69	5.00 (1H, d, 4.8)
15a	76.16	4.42 (1H, dd, 10.2, 6.2)	76.15	4.45(1H, dd, 10, 6.8)
15b	76.16	4.13 (1H, dd, 10.2, 1.4)	76.15	4.13 (1H, d 10)
16	172.65	-	174.67	
17a	109.24	4.85 (1H, s)	109.23	4.88 (1H, s)
17b	109.24	4.63 (1H, s,)	109.23	4.66 (1H, s)
18	23.40	1.18 (3H, s)	23.34	1.22 (1H, s)
19a	65.00	4.09 (1H, d, 11.2)	65.00	4.1 (1H, d, 11.2)
19b	65.00	3.31 (1H, s)	65.00	3.35 (1H, s)
20	15.55	0.71 (3H, s)	15.55	0.75 (3H, s)
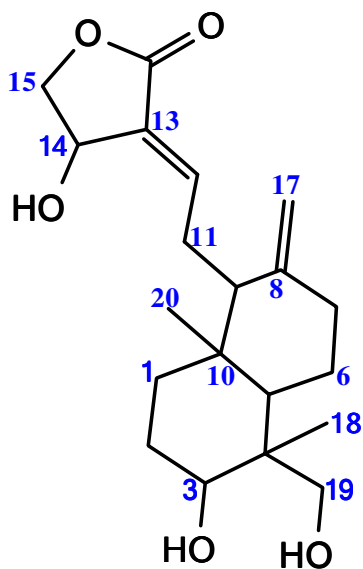
Figure 4.3 Chemical structure of andrographolide
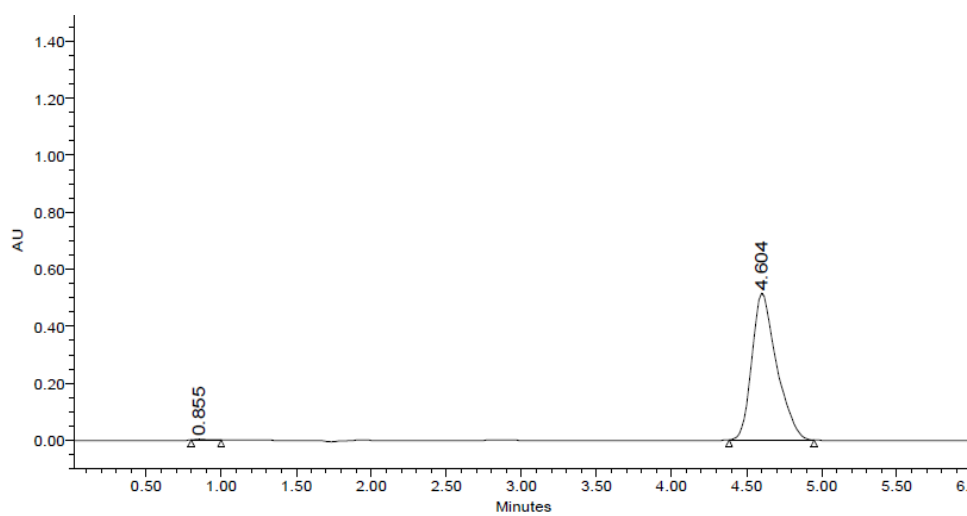
	RT	Area	% Area	Height
1	0.855	9306	0.16	2249
2	4.604	5891504	99.84	514070

Figure 4.4 HPLC chromatograms of the isolated AG

PART II: Synthesis and Characterization of Andrographolidesuccinate grafted chitosan (AGS-*g*-CS)

4.1   Synthesis   of   3,19-Isopropylidene-andrographolide   (2)   and Andrographolide-14-α-*O*-succinate (3)
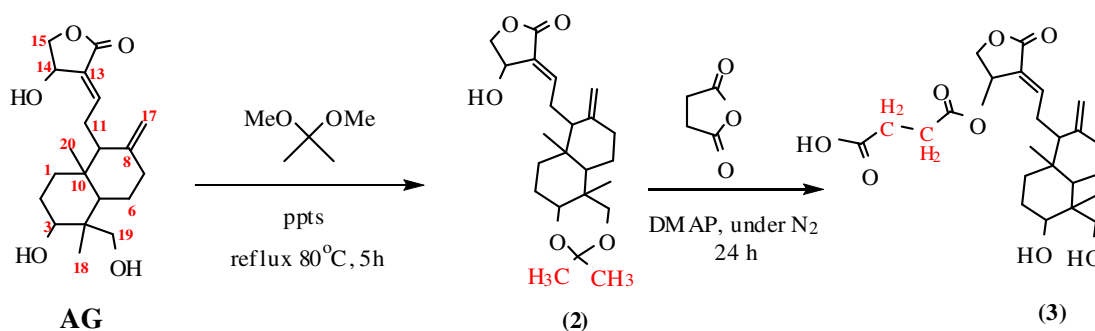
Scheme 4.1 Synthesis of 3,19-isopropylidene-andrographolide (**2**) and andrographolide-14-α-*O*-succinate (**3**)

To synthesize andrographolide-14-α-*O*-succinate (**3**), two hydroxyl groups at C-3 and C-19 of AG (**1**) were firstly protected using 2,2-dimethoxypropane in benzene/DMSO. Succinylation of **2** with succinic anhydride yielded andrographolide-14-α-O-succinate (**3**) after purify by column chromatography. The chemical structures of **2** and **3** were confirmed by ^{1}H-NMR analysis (Figure 4.5). The NMR data of **2** and **3** were in agreement with those of previous report [28].

3,19-Isopropylidene-andrographolide (**2**), ^{1}H NMR (CDCl$_3$, 400 MHz) δ$_H$ 0.95 (3H, s, H-20), 1.19 (3H, s, H-18), 1.36 (3H, s, methyl protons of protecting group), 1.41 (3H, s, methyl protons of protecting group), 2.60-1.24 (12H, methylene and methine protons of AG moiety), 3.19 (1H, d, *J* = 11.6 Hz, H-19b), 3.48 (1H, dd, *J* = 8.8, 3.6 Hz, H-3), 3.97 (1H, d, *J* = 11.6 Hz, H-19a), 4.27 (1H, dd, *J* = 10.4, 2.0 Hz, H-15b), 4.44 (1H, dd, *J* = 10.6, 6.2 Hz, H-15a), 4.61 (1H, s, H-17b), 4.90 (1H, s, H-17a), 5.03 (1H, t, *J* = 6.2 Hz, H-14) and 6.95 (1H, t, *J* = 6.8 Hz, H-12). Two methyl groups at δ 1.36 and 1.41 ppm of the isopropylidene and the separating signals (at δ 3.36-3.31 ppm) of H-3 and H-19 of AG moiety confirmed successful protection of hydroxyl groups (see Figure 4.5b).

Andrographolide-14-α-*O*-succinate (**3**), ^{1}H NMR (CD$_3$OD, 400 MHz) δ$_H$ 0.69 (3H, s, H-20), 1.18 (3H, s, H-18), 2.55-1.25 (12H, methylene and methine protons of AG moiety), 2.59 (4H, s, methylene protons of succinyl moeity), 3.36-3.31 (2H, m, H-3,19b), 4.09 (1H, d, *J* = 11.2 Hz, H-19a), 4.27 (1H, d, *J* = 11.2 Hz, H-15b), 4.56-4.53 (2H, m, H-15a, 17b), 5.99 (1H, d, *J* = 4.4 Hz, H-14) and 6.93 (1H, t, *J* = 6.2 Hz, H-12). The succinate moiety in **3** at C-14 was assured by methylene signals at δ 2.59 ppm together with the downfiled signals of H-14 from δ 5.03 to 5.99 ppm (see Figure 4.5c). Moreover, the methyl proton signals of isopropylidene were disappeared after reacting with succinic anhydride which indicated the deprotection from AG molecule.
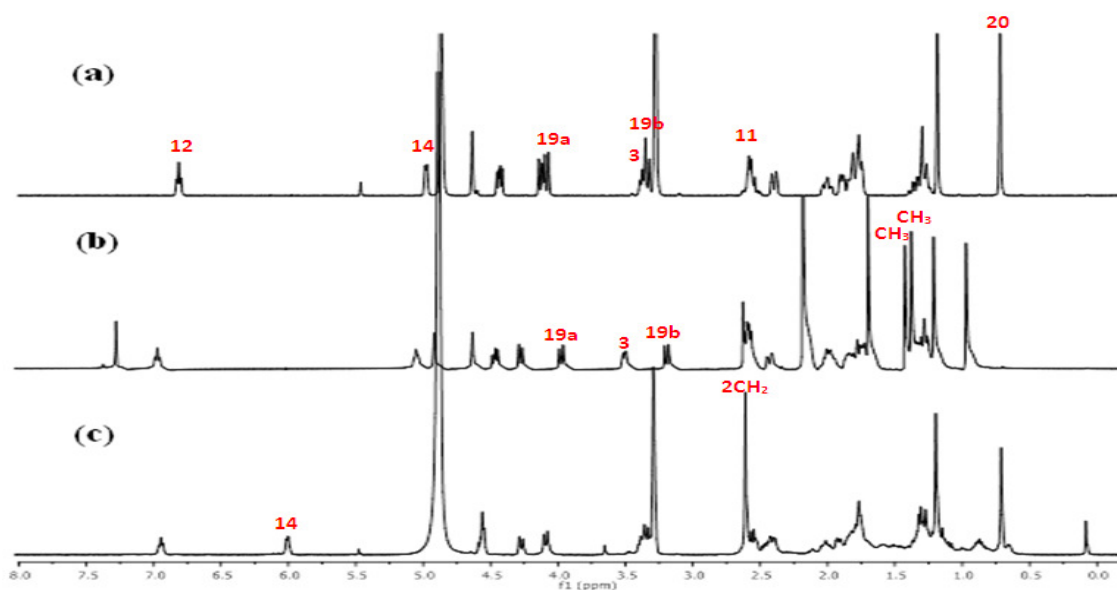
Figure 4.5 ^{1}H NMR spectra of: (a) AG (**1**), (b) 3,19-isopropylidene-andrographolide (**2**) and (c) andrographolide-14-α-O-succinate (**3**)

4.2 Synthesis and Characterization of Andrographolidesuccinate grafted chitosan (AGS-*g*-CS, 4)
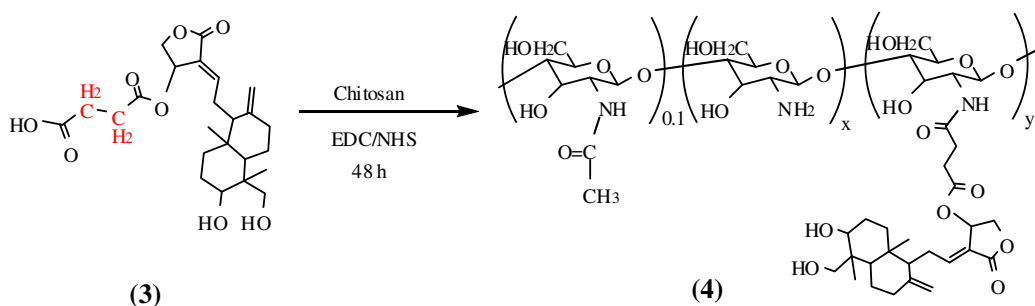
Scheme 4.2 Synthesis of andrographolidesuccinate grafted chitosan

Andrographolide-14-α-*O*-succinate (**3**) was grafted on amino groups of chitosan backbone via amide bond to afford AGS-*g*-CS (**4**). The successful grafting of **3** was confirmed through;

(i) ^{1}H NMR spectrum (D$_2$O-d6, 400 MHz) of **4** appeared the resonance peak at δ = 0.62 (H-20 of AG moiety), 1.22 (H-18 of AG moiety), 2.60-2.40 (methylene protons of succinyl moiety), 2.90 (H-2 of glucosamine, GlcN), 3.50-3.83 (H-2′- of N-acetylglucosamine, GlcNAcm G-3, H-4, H-5 and H-6 of GlcNAc and GlcN) and 4.78 (H-1 of GlcNAc and GlcN). The resonance peak at δ 2.40 and 2.60 ppm were also assigned to methylene protons of the succinyl moiety together with signals of AG moiety (Figure 4.6c.) [59].

(ii) The ATR-FTIR spectrum of **4** (Figure 4.7b.) showed the absorption band at 3360 cm^{-1} (O-H stretching of hydroxyl groups), 2930 (C-H stretching of methyl groups), 1713 (C=O stretching of ester) and 1642 (N-H bending of amide). Thus it could be explained that the absorption band at 1642 cm^{-1} (amide I) increased, indicating that the succinyl moiety took place at the N-position and –NH-CO groups have been formed. Another major change could be observed the increasing band at 2930 cm^{-1} which assigned to carbon-to-hydrogen stretching band (C-H stretching) of methyl groups. Moreover, the absorption band at 1713 cm^{-1} assigned to carbonyl group was increased. Thus confirming that, **3** was substituted [60, 61].
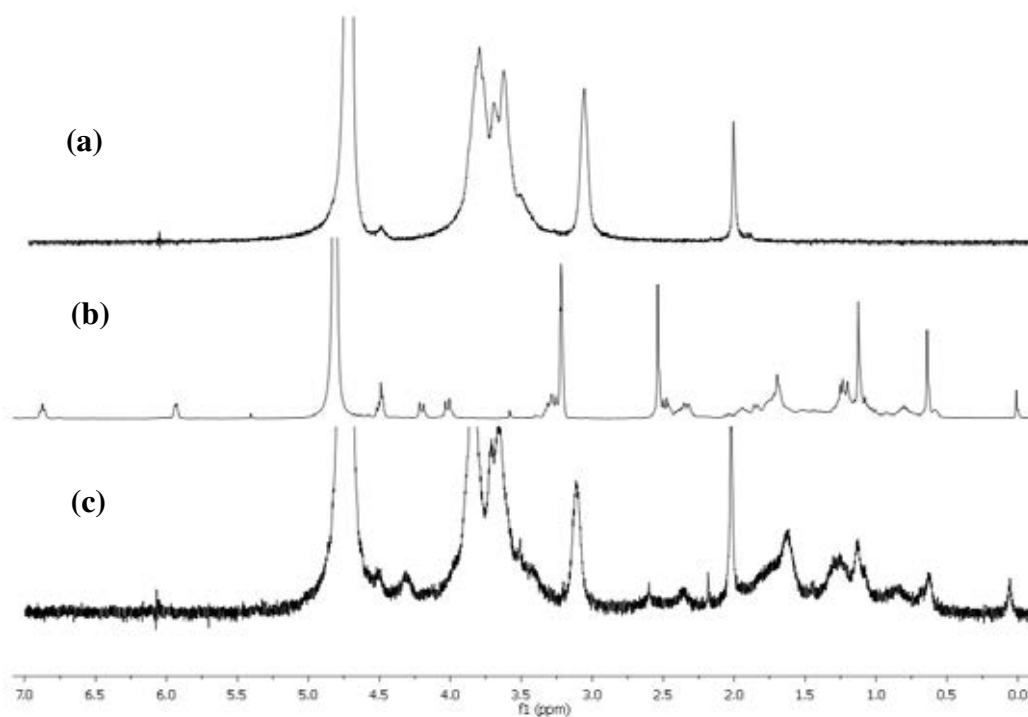
Figure 4.6 ^{1}H NMR spectra of: (a) Chitosan, (b) andrographolide-14-α-*O*-succinate (**3**) and (c) AGS-*g*-CS (**4**)
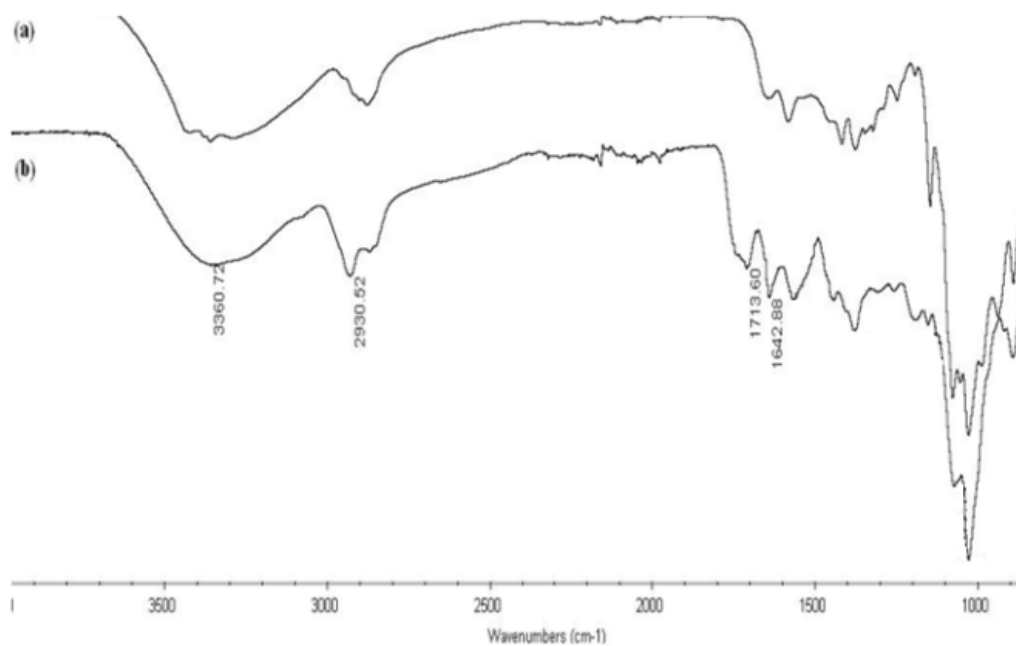
Figure 4.7 FTIR spectra of: (a) Chitosan and (b) AGS-*g*-CS (**4**)

In addition, the product solution (**4**) after dialysis was turned to be a milky solution as shown in Figure 4.8, which indicated that it might be formed self-assembly in the distilled water.
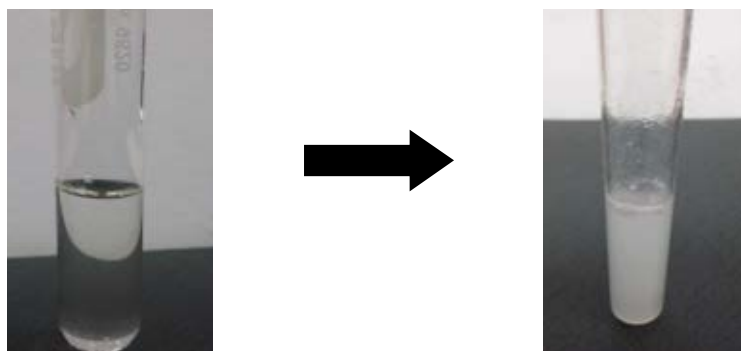
Figure 4.8 a) The solution of AG-*g*-NSCS before dialysis and b) The milky solution of AGS-*g*-CS after dialysis

4.3 The Degree of Substitution

The degree of andrographolide-14-α-*O*-succinate grafting was estimated from the ^{1}H-NMR spectrum using the ratio between the integrated area of the resonance peaks from hydrogen atoms at C-2 in glucosamine units (1H, δ_H 3.14 ppm) and those at C-20 in AG (3H, δ_H 0.62 ppm). The integrated area peak of C-2 in glucosamine units and C-20 in AG were found to be 3.67 and 1, respectively. Taking into account the degree of deacetylation of 0.90 for the starting chitosan, the degree of andrographolide-14-α-*O*-succinyl grafting was approximated to be 0.075 (please see calculation in Appendix A) [59].

However, the amount of AG might be remained in AGS-*g*-CS particles. In order to estimate the ungrafted, AG-*g*-NSCS was immersed in MeOH and filtered by using centrifuge filter. The solution was collected and analyzed by HPLC, and then calculated the ungrafted AG as shown in Appendix B. The calculation result showed that the remained AG in nanoparticles was found to be 0.08%. Therefore, the actual AG could be grafted on chitosan backbone 7.42%. However, the degree of

substitution was reported only two significant number. Thus in this study, the degree of andrographolide-14-α-*O*-succinate substitution was 0.07 as shown in Figure 4.9.
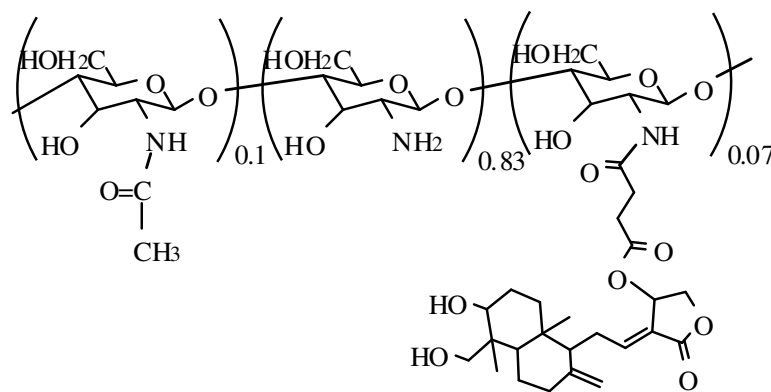
Figure 4.9 Chemical structure of AGS-*g*-CS

4.4 Morphology Study

AGS-*g*-CS could self-assembly in the distill water as describe in Section 4.2. The SEM image of the dried AGS-*g*-CS (Figure 4.10) indicated the spherical morphology with size of 120 ± 2 nm of particles. The hydrodymamic diameter and zeta potential of the hydrated (aqueous suspension) AGS-*g*-CS were 154 ± 2 nm (Polydispersity index, PDI of 0.227 ± 0.005) and +40.33 ± 1   mV, respectively (Figure 4.11). When comparing the average size from both SEM and DLS, it was found that the product gave different values. This might be attributed to the fact that SEM measurement was carried out on dry particles while DLS was carried out directly on aqueous dispersed particles [62]. The high positive zeta potential implied stable dispersion of the particles in water with minimal aggregation [63].

Chitosan is soluble in aqueous acidic medium (pH < 6.5) but insoluble in water due to strong intermolecular hydrogen bonding (H-bond) [10]. Introducing andrographolide-14-α-*O*-succinate onto chitosan backbone probably disrupting the intermolecular H-bond. More importantly, the AGS-*g*-CS was amphiphilic and could automatically self-assemble into stable nanoparticles with the hydrophobic moieties

arranged themselves at the inner core of the particles, away from hydrophilic water, and the hydroxyl groups of chitosan at the outer surface of the particles, with maximum contact with water molecules (Figure 4.12).
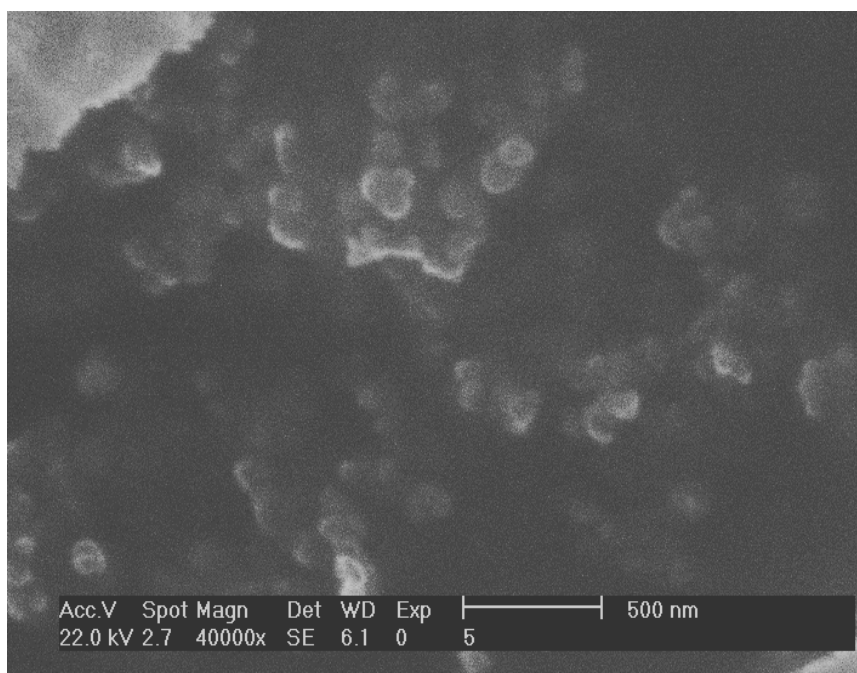
Figure 4.10 SEM image of AGS-*g*-CS spheres
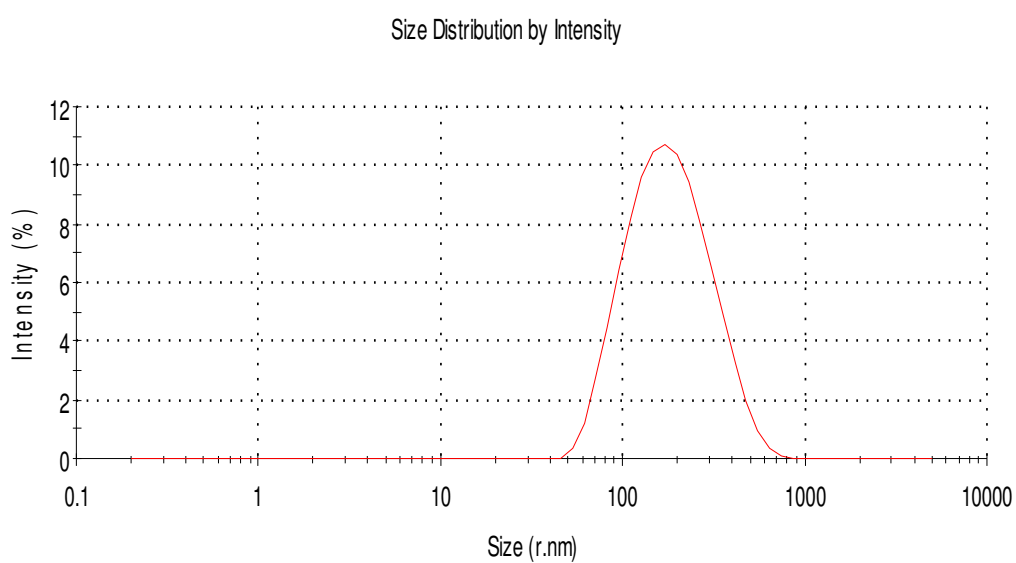
Figure 4.11 Zeta potential distribution graph of AGS-*g*-CS nanoparticles
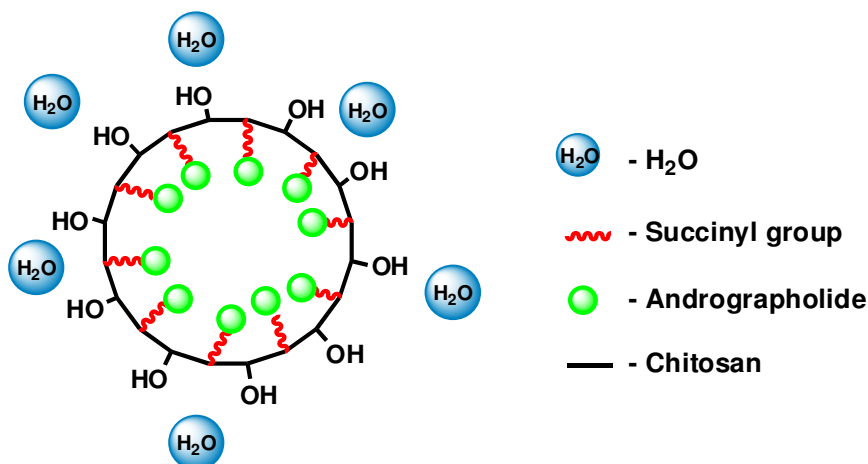
Figure 4.12 Self-assembled structure model of AGS-*g*-CS nanoparticles

4.5 Critical Aggregation Concentration

The critical aggregation concentration (CAC) was estimated to prove the potential of nanoparticles formation of AGS-*g*-CS in distilled water. The CAC of AGS-*g*-CS was defined using fluorescence spectroscopy by observing the assembly of AGS-*g*-CS in the presence of pyrene as a hydrophobic fluorescence probe. The pyrene moved into hydrophobic core, and fluorescence spectra were recorded. Then the ratio of fluorescence emission intensity (I_{382}/I_{372}) was plotted versus the logarithm of AGS-*g*-CS concentrations as shown in Figure 4.13. The emission intensity ratio (I_{382}/I_{372}) was increased significantly when the concentration of polymer was higher than its CAC value, which indicated that nanoparticles could be formed [64]. Hence, the CAC value was evaluated by drawing lines interception between the fitted line at low concentration and fitted line on the rapid rising part of the curve. Thus, the CAC was found to be 0.063 mg/mL. In addition, CAC of AGS-*g*-CS was also significantly lower than the low-molecular weight surfactants (e.g. deoxycholic acid = 1 mg/mL, sodium dodecyl sulfate = 2.3 mg/mL) [64]. Therefore, the result indicated that AGS-*g*-CS might stable in aqueous environment, even after extreme dilution.
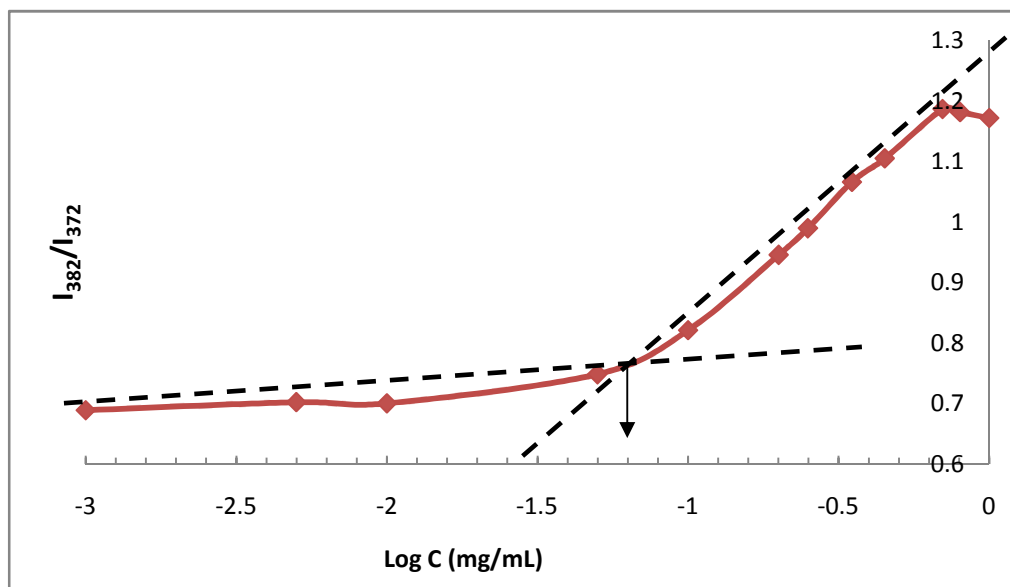
Figure 4.13 Critical aggregation concentration of AGS-*g*-CS in distilled water

4.6 X-ray Diffractometry Analysis (XRD)

X-ray diffraction diagrams of chitosan and AGS-*g*-CS were shown in Figure 4.14. Chitosan gave two intense sharp peaks at 2θ of 10° and 20° (Figure 4.14a), which were attributed to the crystal form. Whereas the AGS-*g*-CS showed a broad 2θ peak (Figure 4.14b) at around 22°. This information suggested that AG-*g*-NSCS was significantly less crystalline than chitosan. This could be presumed that the polymer packing structure changed and hydrogen bonding in chitosan structure decreased by modified the chitosan. Therefore, structure of AG-*g*-NSCS came into view amorphous state and caused the freedom chain to self-assemble into aqueous solution.
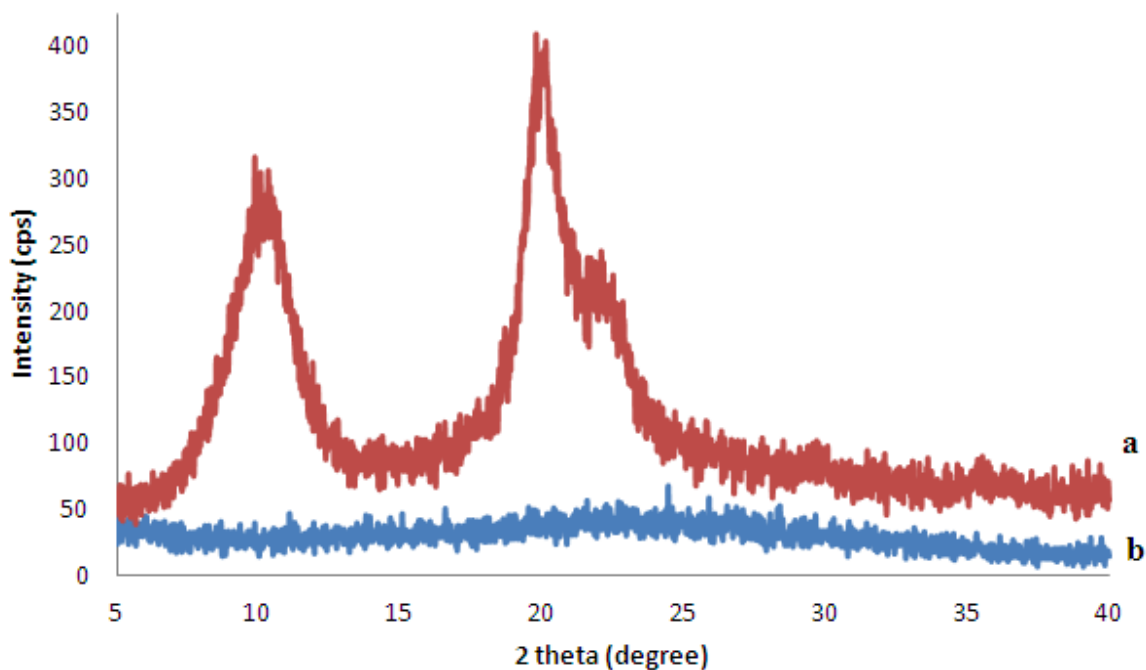
Figure 4.14 X-ray diffraction patterns of: a) chitosan and b) AGS-*g*-CS

4.7 Thermal analysis

The thermal properties of polymer can be explained its mechanical properties, which are related to the chemical structure of polymer. Thus the thermal properties are used to characterize the polymer. This study, the decomposition, glass transition and melting temperature were measured by TGA and DSC.

4.7.1 Thermal Gravimetric Analysis (TGA)

The TGA thermograms of chitosan and AGS-*g*-CS were shown in Figure 4.15. Chitosan showed two decomposition states of weight loss within the range of 50 to 400 °C. The first state appeared in the range 50 to 100 °C, which might be assigned the moisture vaporization and bound water with a weight loss of about 7.2 %. The next state of chitosan thermogram showed that chitosan started to decompose at 225 °C and presented the decomposition temperature (T_d) at 332 °C with 39.1% weight loss.
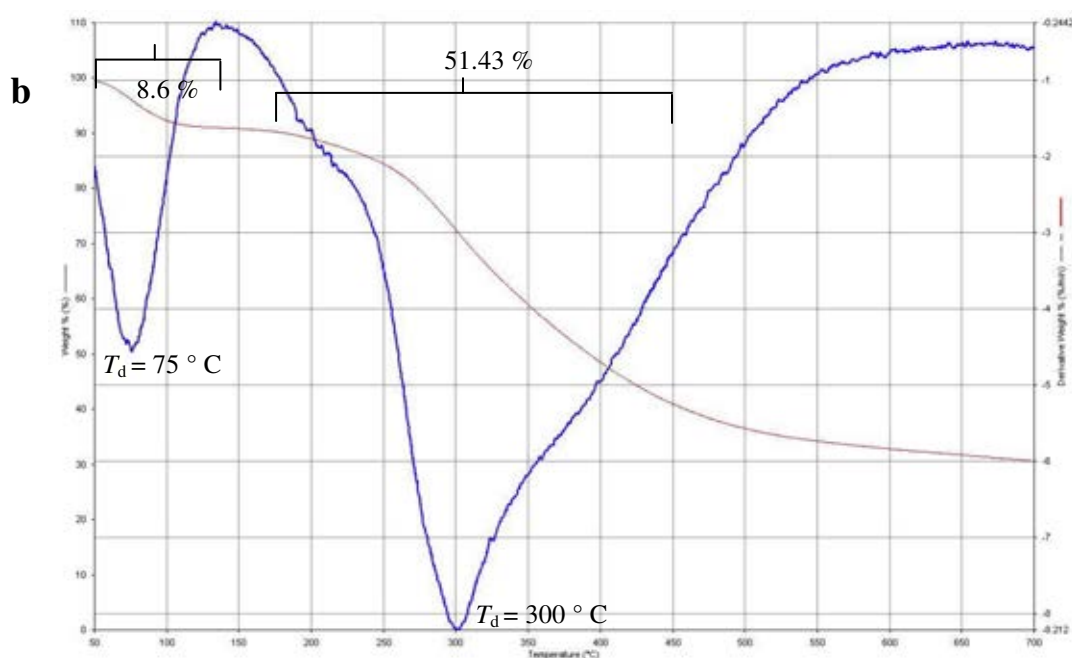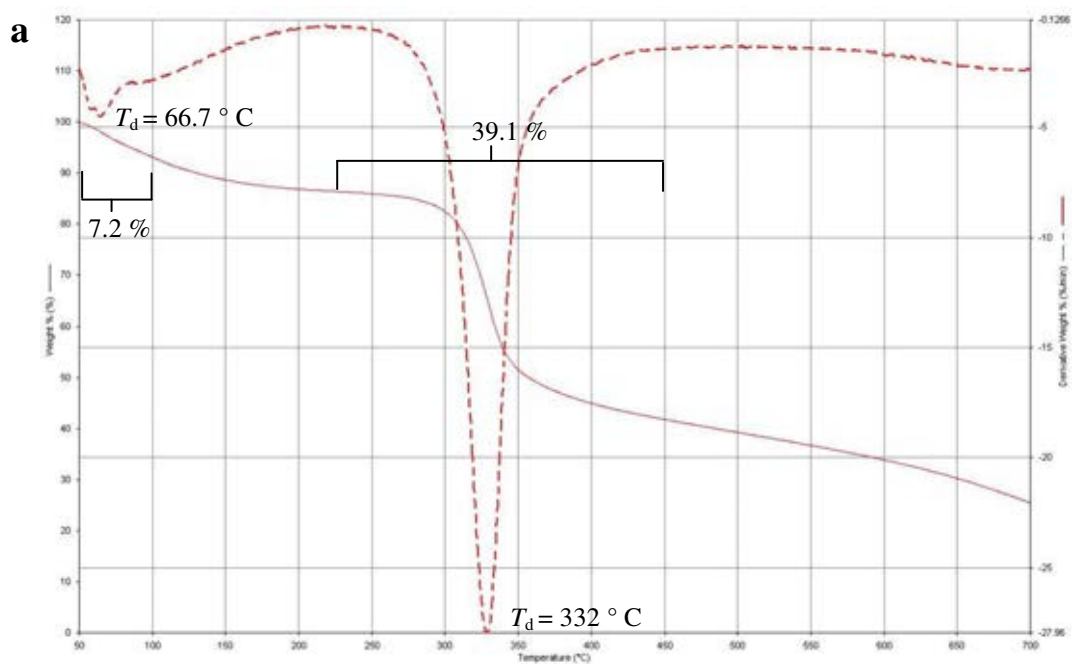
Figure 4.15 TGA thermograms of: a) chitosan and b) AGS-*g*-CS

For the AGS-*g*-CS, the weight loss in two steps within the temperature range of 50 to 450 °C. The first state, the weight was lost in the range of 50 to 130 °C, ascribed to evaporation of moisture with a weight loss of about 8.6 %, this result found that the water in AGS-*g*-CS has higher evaporation temperature than chitosan. It could be described by the decrease of chitosan crystallinity after grafting andrographolide-14-α-*O*-succinate which was a hydrophobic side chain [65]. The water molecules could penetrate inside the AGS-*g*-NSCS more easily. Moreover, the second weight loss of AGS-*g*-CS appeared in the range of 172 to 450 °C with 51.43 % of weight loss, which was due to the thermal degradation of chitosan and andrographolide-14-α-*O*-succinate. Furthermore, the decomposition temperature (T*d*) of AGS-*g*-CS was found to be 300 °C, T_d of AGS-*g*-CS was lower when compared to chitosan. Thus, this result indicated that AGS-*g*-CS was lower thermal stability than chitosan because andrographolide-14-α-*O*-succinate groups interfered with the close packing between the molecules of chitosan. Therefore, this thermal analysis results corresponded to the results of X-ray diffractometry analysis.

4.7.2 Differential Scanning Calorimetry Analysis (DSC)

The diffrerential scanning calorimetry thermograms of chitosan and AGS-*g*-CS were characterized by two thermal events: the first was an endothermic peak and the second was an exothermic peak. The spectra of chitosan (Figure 4.16a) showed a broad endothermic peak at 93.1 °C in the first range (29 - 130°C) corresponding to the loss of water and moisture in chitosan. While the sharp exothermic peak at 307.1 °C in the range of280 - 330°C was associated with the decomposition of chitosan chain. For the AGS-*g*-CS (Figure 4.16b), the endothermic peak at 91.5 °C might be due to the water vapor in AGS-*g*-CS. The broad exothermic peak at 268 °C in the range of 230 – 285 °C attributed to the thermal degradation of AGS-*g*-CS. This result indicated that the AGS-*g*-CS was less stable than chitosan due to its lower degradation temperature. This might be the decreasing crystallization of chitosan structure. However, the AGS-*g*-CS did not showed glass transition temperature.

From XRD and thermal analysis (TGA and DSC), we can conclude that chitosan was modified and changed its structure from crystalline form to amorphous form causing the AGS-*g*-CS was less thermal stable than chitosan.
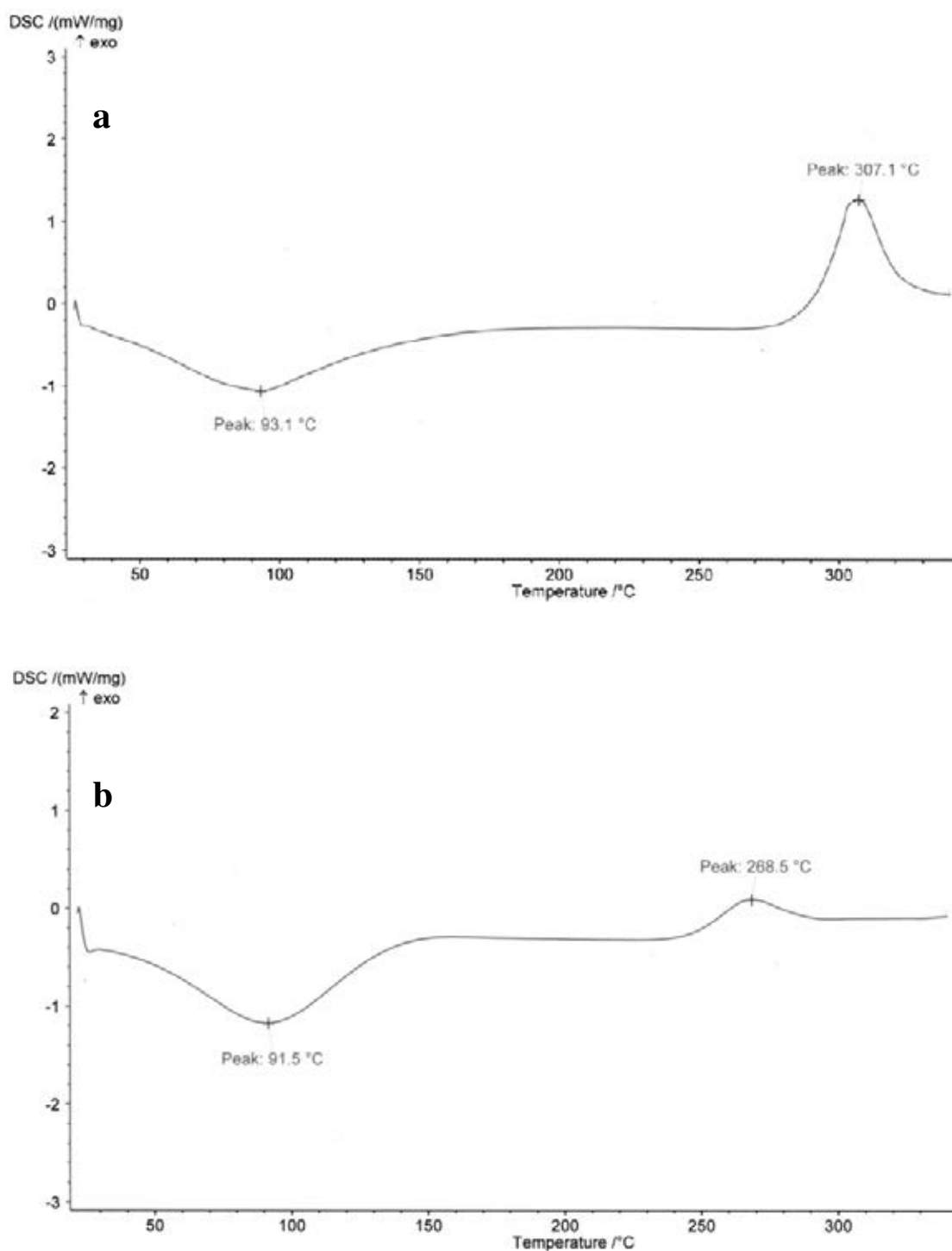
Figure 4.16 DSC thermograms of: a) chitosan and b) AGS-*g*-CS

4.8 Cytotoxicity Study (MTT assay)

AG has a wide spectrum of pharmacological properties including anti-cancer activity. In this study, andrographolide-14-α-*O*-succinate was grafted onto chitosan expecting to obtain the chitosan derivative (AGS-*g*-CS) which has anti-cancer activity. Thus, anti-cancer activities of AGS-*g*-CS, AG and andrographolide-14-α-*O*-succinate were evaluated using MTT assay.

Cytotoxicity activities of AGS-*g*-CS towards breast cancer (MCF-7) and cervical cancer (CaSki) cell lines were summarized in Table 4.2. The IC_{50} values in Table 4.2 is the concentration of AG in the sample that can inhibit cell lines 50%. The IC_{50} values for AG in AGS-*g*-CS towards cervial and breast cancer cell lines were 9.66 and 3.59 µg/mL, respectively, which lower than those of free AG (IC_{50} = 16.34 and 7.10 µg/mL, respectively). The reason for enhacing activity of AGS-*g*-CS might be studied in the future. Therefore, AGS-*g*-CS nanoparticle has great potential to be used as a novel drug carrier.

Table 4.2 Anticancer activity of andrographolide (AG), andrographolide-14-α-*O*-succinate (AG-Suc) and AGS-g-CS towards cervical and breast cancer cell lines.

Samples	IC_{50} (µg/mL)	
	Cervical cancer	Breast cancer
AG	16.34	7.10
AG-Suc	Not active	>50
AGS-g-CS	9.66	3.59

CHAPTER V

CONCLUSION

In this study andrographidesuccinate grafted chitosan (AGS-*g*-CS) is successfully synthesized. The chemical structures are characterized by ^{1}H NMR and FTIR analysis with the degree substitution of andrographolide-14-α-*O*-succinate 7.42% (Figure 5.1).
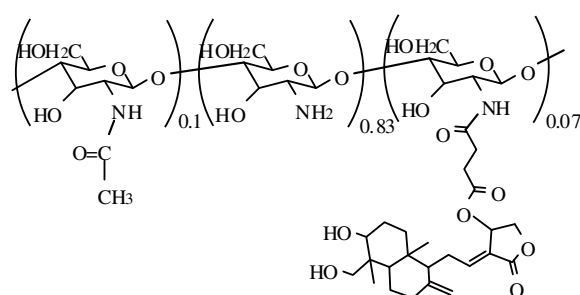
Figure 5.1 Chemical structure of AGS-*g*-CS

Moreover, AGS-*g*-CS can be self-assembled to be nanoparticles (Figure 5.2) at critical agreegation concentration (CAC) of 0.063 mg/mL indicating that AGS-*g*-CS was stable in the diluted water. These particles have the spherical shape with the average size of 154 ± 2 nm in distilled water.
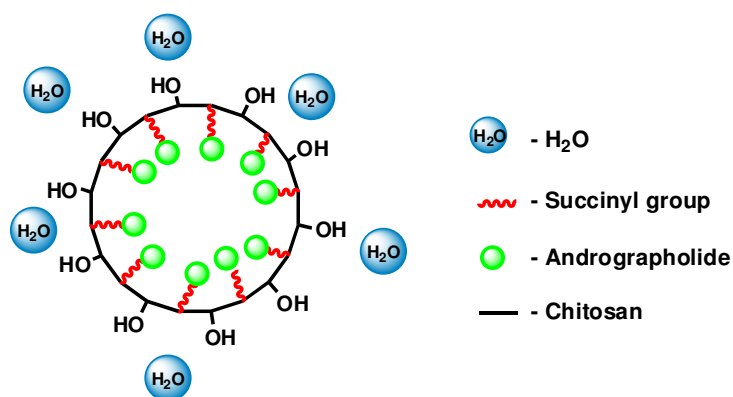
Figure 5.2 Self-assembled structure model of AG-*g*-NSCS nanoparticles

Furthermore, the crystal property of AGS-*g*-CS is studied by XRD. The crystalline form of chitosan is changed to amorphous form when grafting andrographolide-14-α-*O*-succinate on chitosan backbone. In addition, AGS-*g*-CS is lower thermal stability than chitosan because andrographolide-14-α-*O*-succinate groups interfered with the close packing between the molecules of chitosan. Therefore, these thermal analysis results corresponded to the results of X-ray diffractometry analysis.

Finally, the cytotoxicity of AGS-*g*-CS is studied. The IC_{50} values for AG in AGS-*g*-CS towards cervial and breast cancer cell lines were lower than those of free AG. The reason for enhacing activity of AGS-*g*-CS might be studied in the future. Therefore, AGS-*g*-CS nanoparticle has great potential to be used as a novel drug carrier.

REFERENCES

[1] Park, J.H., Saravanakumar, G., Kim, K. and Kwon, I.C. Targeted delivery of low molecular drugs using chitosan and its derivatives. <u>Advanced Drug Delivery Reviews</u>. 62 (2010): 28-41.

[2] Tiyaboonchai, W. Chitosan nanoparticles : a promising system for drug delivery. <u>Naresuan University Journal</u>. 11 (2003): 51-66.

[3] Letchford, K. and Burt, H. A review of the formation and classification of amphiphilic block copolymer nanoparticulate structures: micelles, nanospheres, nanocapsules and polymersomes. <u>Drug delivery: a Canadian perspective</u>. 66 (2007): 259-269.

[4] Rosen, H. and Abribat, T. The rise and rise of drug delivery. <u>Nature Review Drug Discovery</u>. 4 (2005): 381-385.

[5] Ajazuddin and Saraf , S. Applications of novel drug delivery system for herbal formulation. <u>Fitoterapia</u>. 81 (2010): 680–689.

[6] Tong, R. and Cheng, J. Anticancer Polymeric Nanomedicines. <u>Polymer Reviews</u>. 47 (2007): 345-381.

[7] Duncan, R. Polymer conjugates as anticancer nanomedicines. <u>Natural review/cancer</u>. 6 (2006): 688-701.

[8] Sokolsky-Papkov, M., Agashi, K., Olaye, A., Shakesheff, K. and Domb, A. J. Polymer carriers for drug delivery in tissue engineering. <u>Advanced Drug Delivery </u>Reviews. 59 (2007): 187–206.

[9] Liu, Z., Jiao, Y., Wang, Y., Zhou, C. and Zhang, Z. Polysaccharides-based nanoparticles as drug delivery systems. <u>Advanced Drug Delivery Reviews</u>. 60 (2008): 1650–1662.

[10] Rinaudo, M. Chitin and chitosan: Properties and applications. <u>Progress in Polymer Science</u>. 31 (2006): 603-632.

[11] Yan, C., Chen, D., Gu, J., Hu, H., Zhao, X. and Qiao, M. Preparation of N-succinyl-chitosan and its physical-chemical properties as a novel excipient. <u>The phamaceutical Society of Japan</u>. 126(9) (2006): 789-793.

[12] Aiping, Zhu., Tian C., Lanhua Y., Hao W., and Ping, L. Synthesis and characterization of *N*-succinyl-chitosan and its self-assembly of nanospheres. Carbohydrate Polymers. 66 (2006): 274–279.

[13] Xia, W., Liu, P., Zhang, J. and Chen, J. Biological activities of chitosan and chitooligosaccharides. Food Hydrocolloids. (2010): 1-10.

[14] Denkbas, E.B. and Ottenbrite, R.M. Perspectives on: Chitosan Drug Delivery Systems Based on their Geometries. Journal of Bioactive and Compatible Polymers. 21 (2006): 351-367.

[15] Denkbas, E.B. and Ottenbrite, R.M. Perspectives on: Chitosan Drug Delivery Systems Based on their Geometries. Journal of Bioactive and Compatible Polymers. 21 (2006): 351-367.

[16] Ngawhirunpat, T., Wonglertnirant N., Opanasopit, P., Ruktanonchai, U., Yoksan, R., Wasanasuk, K. and Chirachanchai, S. Incorporation methods for cholic acid chitosan-g-mPEG self-assembly micellar system containing camptothecin. Colloids and Surfaces B: Biointerfaces. 74 (2009): 253–259.

[17] Zhao, Z., He M., Yin, L., Bao, J., Shi, L., Wang, B., Tang, C. and Yin, C. Biodegradable nanoparticles based on linoleic acid and poly(beta-malic acid) double grafted chitosan derivatives as carriers of anticancer drugs. Biomacromolecules. 10 (2009): 565–572.

[18] Kato, Y., Onishi, H. and Machida, Y. *N*-succinyl-chitosan as a drug carrier:water-insoluble and water-soluble conjugates. Biomaterials. 25 (2004): 907–915.

[19] Hou, Z. Q., Han, J., Zhan, C. M., Zhou, C. X., Hu, Q. A., and Zhang, Q. Q. Synthesis and evaluation of N-succinyl-chitosan nanoparticles toward local hydroxycamptothecin delivery. Carbohydrate Polymers. 81 (2010): 765–768.

[20] Luo, H., Li, J. and Chen, X. Antitumor effect of N-succinyl-chitosan nanoparticles on K562 cells. Biomedicicene & Phamacotherapy. 64 (2010): 521-526.

[21] Rando, D. G., Brandt, C. A. and Ferreira, E. I. Use of N-methylene phosphonic chitosan to obtain an isoniazid prodrug. Brazilian Journal of Pharmaceutical Sciences. 40 (2004): 335-344.

[22]   Mura, C., Manconi, M., Valenti D., Manca, M. L., Diez-Sales O., Loy, G. and Fadda, A. M. In vitro study of N-succinyl chitosan for targeted delivery of 5-aminosalicylic acid to colon. <u>Carbohydrate Polymers</u>. 85 (2011) 578–583.

[23]   Toh, E. K.-W., Chen H.-Y., Lo, Y.-L., Huang, S.-J. and Wang, L.-F. Succinated chitosan as a gene carrier for improved chitosan solubility and gene transfection. <u>Nanomedicine: Nanotechnology, Biology, and Medicine</u>. 7 (2011): 174–183.

[24]   Song, Y., Onishi, H., Machida, Y. and Nagai, T. Drug release and antitumor characteristics of N-succinyl-chitosan-mitomycin C as an implant. <u>Journal of Controlled Release</u>. 42 (1996): 93–100.

[25]   Kato, Y., Onishi, H. and Machida, Y. Biological characteristics of lactosaminated N-succinyl-chitosan as a liver-specific drug carrier in mice. <u>Journal of Controlled Release</u>. 70 (2001): 295–307.

[26]   Wang, Y.-S., Liu, L.-R., Jiang, Q. and Zhang, Q.-Q. Self-aggregated nanoparticles of cholesterol-modified chitosan conjugate as a novel carrier of epirubicin. <u>European Polymer Journal</u>. 43 (2007): 43–51.

[27]   Chien, C.-F., Wu, Y.-T., Lee, W.-C., Lin, L.-C. and Tsai, T.-H. Herb–drug interaction of Andrographis paniculata extract and andrographolide on the pharmacokinetics of the ophylline in rats. <u>Chemico-Biological Interactions</u>. 184 (2010): 458–465.

[28]   Das, B., Chowdhury, C., Kumar, D., Sen, R., Roy, R., Das, P. and Chatterjee, M. Synthesis, cytotoxicity, and structure–activity relationship (SAR) studies of andrographolide analogues as anti-cancer agent. <u>Bioorganic & Medicinal Chemistry Letters</u>. 20 (2010): 6947–6950.

[29]   Aguiar, J., Carpena, P., Molina-Bolívar, J.A. and Carnero Ruiz, C. On the determination of the critical micelle concentration by the pyrene 1:3 ratio method. <u>Journal of Colloid and Interface Science</u>. 258 (2003): 116–122.

[30]   Nunthanawanit, P. Targeted prodrugs. <u>Thai Pharmaceutical and Health Science Journal</u>. 5(3) (2010): 270-278.

[31]   Mitragotri, S. Recent Advances in Novel Drug Delivery Systems. <u>Frontiers of Engineering</u>. 38 (2008): 5-12.

.

[32] Edlund, U. and Albertsson, A. C. Degradable polymer microspheres for controlled drug delivery. Advances in polymer science. 157(2002): 68-91.

[33] Sinha, R., Kim, G. J., Nie S. and Shin, D. M. Nanotechnology in cancer therapeutics: bioconjugated nanoparticles for drug delivery. Molecular Cancer Therapeutics. 5 (2006): 1909-1917.

[34] Lincoln, P. Targeted drug delivery. White Rose HIP Health Technology Bulletins.

[35] Nair, H.B., Sung, B., Yadav, V.R., Kannappan, R., Chaturvedi, M.M. and Aggarwal, B.B. Delivery of anti-inflammatory nutraceuticals by nanoparticles for the prevention and treatment of cancer. Biochem Pharmacol. 80 (2010): 1833-1843.

[36] Mishra, B., Patel B. B. and Tiwari S. Colloidal nanocarriers: a review on formulation technology, types and applications toward targeted drug delivery. Nanomedicine: Nanotechnology, Biology, and Medicine. 6 (2010): 9–24.

[37] Ringdorf, H. Structure and properties of pharmacologically active polymers. Journal of Polymer Science. 51 (1975): 135–53.

[38] Ranade, V.V. and Cannon J.B. Role of Polymer in Drug Delivery. Drug delivery systems. (2011): 1-513.

[39] Ranade, V.V. and Cannon J.B. Role of Polymer in Drug Delivery. Drug delivery systems. (2011): 1-513.

[40] Sonia, T.A. and Sharma C.P.Chitosan and Its Derivatives for Drug Delivery Perspective. Advance in Polymer Science. (2011) 243: 23–54.

[41] Sashiwa, H. and Aiba S. Chemically modified chitin and chitosan as biomaterials. Progress in Polymer Science. 29 (2004) 887–908.

[42] Yamaguchi, R., Arai, Y., Itoh, T. and Hirano, S. Preparation of partially N-succinylated chitosans and their cross-linked gels. Carbohydrate Research. 88 (1981): 172-175.

[43] Kato, Y., Onishi, H. and Machida, Y. Depolymerization of N-succinylchitosan by hydrochloric acid. Carbohydrate Research. 337 (2002): 561-564.

[44]   Kuroyanagi, Y., Shiraishi, A., Shirasaki, Y., Nakakita, N., Yasutomi. Y., Takano, Y. and Shioya, N. Development of a new wound dressing with antimicrobial delivery capability. Wound Repair Regen. 2 (1994): 122-129.

[45]   Kato, Y., Onishi, H. and Machida, Y. Evaluation of N-succinyl-chitosan as a systemic long-circulating polymer. Biomaterials. 21 (2000): 1579-1585.

[46]   Chao, W.-W. and Lin, B.-F. Isolation and identification of bioactive compounds in *Andrographis paniculata* (*Chuanxinlian*). Chinese medicine. 5 (2010): 1-15.

[47]   Jada, S. R., Subur, G. S., Matthews, C., Hamzah, A. S., Lajis, N. H., Saad, M. S., Stevens, M.F.G. and Stanslas, J. Semisynthesis and *in vitro*anticancer activities of andrographolide analogues. Phytochemsitry. 68 (2007): 904–912.

[48]   Anju, D., Jugnu, G., Kavita, S., Arun, N. and Sandeep, D. A review on medicinal prospective of *Andrographhis paniculata* NEES. Journal of Pharmaceutical and Scientific Innovation. 1(2012): 1-4.

[49]   Kumoro, A. C. and Hasan, M. Experimental and Modeling Studies of Andrographolide Extraction from Andrographis paniculata in a Soxhlet Extractor. Project No. F0125/2004D.

[50]   Savjani, K.T., Gajjar, A.K. and Savjani J.K. Drug Solubility: Importance and Enhancement Techniques. International Scholarly Research Network. (2012): 1-10.

[51]   Onlaor, S. Microencapsulation of *Andrographis Paniculata* Nee Extract for Suxtainedrelease by Solvent Evaporation Technique. 187.

[52]   Zhao, D., Liao, K., Ma X. and Yan, X. Study of the Supramolecular Inclusion of *β*-Cyclodextrin with Andrographolide. Journal of Inclusion Phenomena and Macrocyclic Chemistry. 43 (2002): 259–264.

[53]   Kumar, R. A., Sridevi, K., Kumar, N. V., Nanduri, S. and Rajagopal, S. Anticancer and immunostimulatory compounds from. Andrographis paniculata**. Journal of Ethnopharmacology. 92 (2004): 291-295.

[54]   Chen, L., Zhu, H., Wang, R., Zhou, K., Jing, Y. and Qiu, F. *ent*-Labdane diterpenoid lactone stereoisomers from *Andrographis paniculata***. Journal of Natural Products. 71 (2008): 852-855.

[55]   Shi, M.-D., Lin, H.-H., Lee, Y.-C., Chao, J.-K., Lin, R.-A. and Chen, J-H. Inhibition of cell-cycle progression in human colorectal carcinoma Lovo cells by andrographolide. <u>Chemico-Biological Interactions</u>. 174 (2008): 201–210.

[56]   Yang, L., Wu, D., Luo, K., Wu, S. and Wu, P. Andrographolide enhances 5-fluorouracil-induced apoptosis via caspase-8-dependent mitochondrial pathway involving p53 participation in hepatocellular carcinoma (SMMC-7721) cells. <u>Cancer Letters</u>. 276 (2009): 180–188.

[57]   Huo, M., Zhang, Y., Zhou, J., Zou, A., Yu, D., Wu, Y., Li, J. and Li, H. Synthesis and characterization of low-toxic amphiphilic chitosan derivatives and their application as micelle carrier for antitymor drug. <u>International Journal of Pharmaceutics</u>. 394 (2010): 162-173.

[58]   Sahu, A., Bora, U., Kasoju, N. and Goswami, P. Synthesis of novel biodegradable and self-assembling methoxy poly(ethylene glycol)-palmitate nanocarrier for curcumin delivery to cancer cells. <u>Acta Biomaterialia</u>. 4 (2008): 1752-1761.

[59]   Tree-udom, T., Wanichwecharungruang, S.P. and Seemork, J. Fragrant chitosan nanospheres: Controlled release systems with physical and chemical barriers. <u>Carbohydrate Polymers</u>. 86 (2011): 1602-1609.

[60]   Zhou, J.Q. and Wang, J.W. Immobilization of alliinase with a water soluble-insoluble reversible N-succinyl-chitosan for allicin production. Enzyme and Microbial Technology. 45 (2009): 299–304.

[61]   Xiangyang, X., Ling, L., Jianping, Z., Shiyue, L., Jie, Y., Xiaojin, Y. and Jinsheng, R. Preparation and characterization of *N*-succinyl-*N'*-octyl chitosan micelles as doxorubicin carriers for effective anti-tumor activity. <u>Colloids and Surfaces B: Biointerfaces</u>. 55 (2007): 222-228.

[62]   Lao, S.-B., Zhang, Z.-X., Xu, H.-H. and G.-B. Jiang, Novel amphiphilic chitosan derivatives: Synthesis, characterization and micellar solubilization of rotenone. <u>Carbohydrate Polymers</u>. 82 (2010): 1136-1142.

[63]   Kwon, S., Park, J.H., Chung, H., Kwon, I.C., Jeong, S.Y. and Kim, I.-S. Synthesis and characterization of sugar-bearing chitosan derivatives:

aqueous solubility and biodegradability. <u>Langmuir</u>. 19 (2003): 10188-10193.

[64] Huo, M., Zhang, Y., Zhou, J. Zou, A., Yu, D., Wu, Y. Li, J. and Li, H. Synthesis and characterization of low-toxic amphiphilic chitosan derivatives and their application as micelle carrier for antitumor drug. <u>International Journal of Pharmaceutics</u>. 394 (2010): 162-173.

[65] Qu, X., Wirsén, A., Albertsson, A.-C. Novel pH-sensitive chitosan hydrogels: swelling behavior and states of water. <u>Polymer</u>. 41 (2000): 4589-4598.

APPENDICES

Appendix A

Determination of degree substitution

The degree of andrographolide-14-α-*O*-succinate grafting on chitosan was estimated from the ^{1}H-NMR spectrum (Figure A1) using the ratio between the integrated area of the resonance peaks from hydrogen atoms at C-2 in glucosamine units (δ 3.14 ppm) and those at C-20 in AG (δ 0.62 ppm). Moreover, succinylation was evaluated using the integrated area of succinyl moiety at δ 2.4 and 2.6 ppm.

From table A1, the ratio of chitosan : AG : succinyl were calculated to be 11 : 1 : 1.12, it means that the AGS-*g*-CS contained the 8.32 % (equation **1**) of AG. When taking into account the degree of deacetylation of 0.90 for the starting chitosan, the degree of andrographolide-14-α-*O*-succinyl grafting was approximated to be 0.075 or 7.5% (equation **2**). Thus the molecular weight of AGS-*g*-CS was found to be 29880 g/mol (equation **4**). Therefore, 1 mol of AGS-*g*-CS included 3937.5 g of AG (equation **5**).
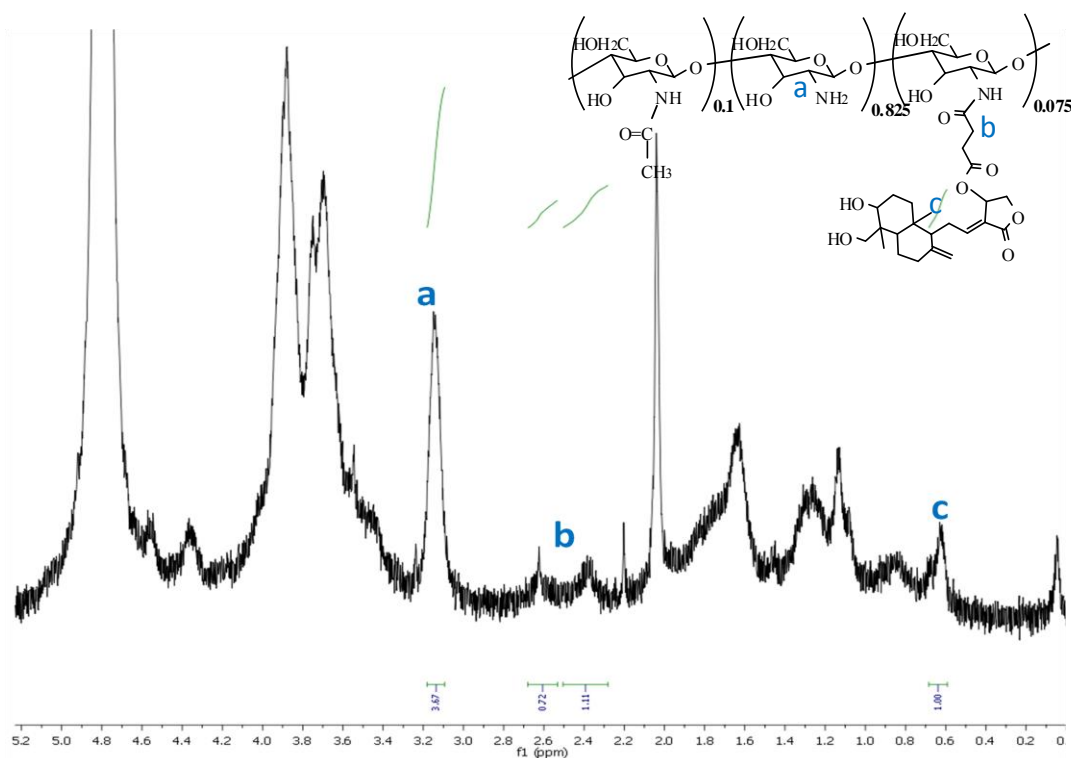

Figure A1 ^{1}H NMR spectrum of AGS-*g*-CS

Table A1 The ratio of ^{1}H NMR area peak of chitosan : AG : succinyl

	Chitosan	AG	Succinyl
Area peak	3.67	1.00	1.50
Number of protons	1	3	4
Area peak/ Number of protons	3.67	0.333	0.375
Simplified further	11.02	1.00	1.12

From table A1, the percentage of grafting andrographolide-14-α-*O*-succinate could be calculated followed as;
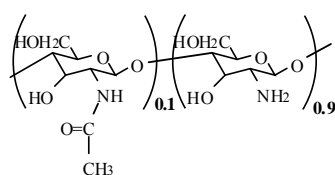
$$\frac{100\% \times Simplified\ further\ of\ AG}{(Simplified\ further\ of\ Chitosan + Simplified\ further\ of\ AG\ )} = \frac{100\% \times 1}{(11.02 + 1)} = 8.32\% \ldots\ldots(1)$$

When taking into account the degree of deacetylation of 0.90;

$$8.32\% \times 0.9 = 7.5\ \% \ldots\ldots\ldots\ldots\ldots\ldots(2)$$

Moreover, molecular weight of AGS-*g*-CS could be calculated by following equation;

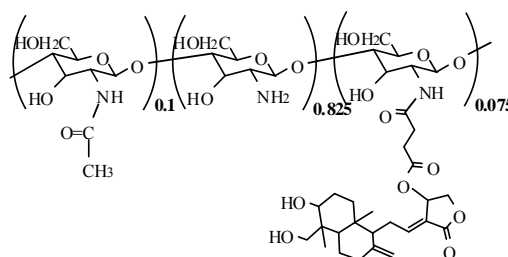1) To find the amount of units of chitosan;

$$x[(DD \times Mw_{glucosamine}) + (DA \times Mw_{glucosamine\ grafted\ acetyl}) = Mw_{Chitosan} \quad (3)$$

Where x was amount of units of chitosan, DD was degree of deacetylation and DA was degree of acetylation.

$$\text{Thus;} \qquad x[(0.9 \times 161) + (0.1 \times 219)] = 25000$$

$$x = 150$$

2) To find the molecular weight of AGS-g-CS;

$$x[(DD \times Mw_{glucosamine}) + (DA \times Mw_{glucosamine\ grafted\ acetyl}) + (DS \times$$
$$Mw_{glucosamine\ grafted\ AG)}] = Mw_{AG-g-NSCS} \cdots\cdots\cdots\cdots\cdots\cdots\cdots\cdots\cdots\cdots\cdots\cdots\cdots\cdots (4)$$

Where x was amount of units of chitosan, DD was degree of deacetylation, DA was degree of acetylation and DS was degree substitution of AG.

$$\text{Thus; } 150[(0.825 \times 161) + (0.1 \times 219) + (0.075 \times 593)] = Mw_{AG-g-NSCS}$$
$$Mw_{AG-g-NSCS} = 29880$$

3) To find amount of AG in 1 mol of AGS-g-CS (29880 g);
$$amount\ of\ AG = Mw_{AG} \times DS \times x$$

Where x was amount of units of chitosan and DS was degree substitution of AG.

$$\text{Thus;} \qquad amount\ of\ AG = 350 \times 0.075 \times 150 = 3937.5g \cdots\cdots\cdots (5)$$

Appendix B

Calculation of the remained AG in AGS-*g*-CS nanoparticles

From part II, the free AG might be remained in the AGS-*g*-CS nanoparticles, which did not graft onto chitosan backbone. The amount of free AG could be obtained from directly measuring the HPLC area peak of free AG in MeOH and then determined the amount of free AG from a calibration curve of free AG in MeOH (Figure B1). In the releasing experiment, the 5.7 mg of freeze dried AGS-*g*-CS was immersed in MeOH (5.7 mL) for 1 day and then filtered the AGS-*g*-CS by centrifuge filter. The solution was collected and evaluated the area by HPLC. The HPLC chromatogram was shown in figure B1, the area peak of free AG (R_t = 4.479 min) was found to be 55123. From the equation of the calibration curve, the remained AG was calculated to be 1.366 ppm (mg/L). Thus the amount of free AG was found to be 0.0078 mg in 5.7 mL of MeOH.

The total amount of AG in AGS-*g*-CS was approximated to be 0.075 by ^{1}H NMR analysis (Appendix A). The molecular weight of AGS-*g*-CS was found to be 29880 g/mol, which contained 3937.5 g of AG. Thus the 5.7 mg of AGS-*g*-CS included the 0.751 mg of AG. Therefore, the substituted AG on chitosan backbone could be calculated by the subtraction of the total amount of AG (from NMR analysis) and the free AG (from HPLC), it was found to be 0.7433 mg . The actual grafted AG on chitosan backbone was calculated to be 7.42 %.
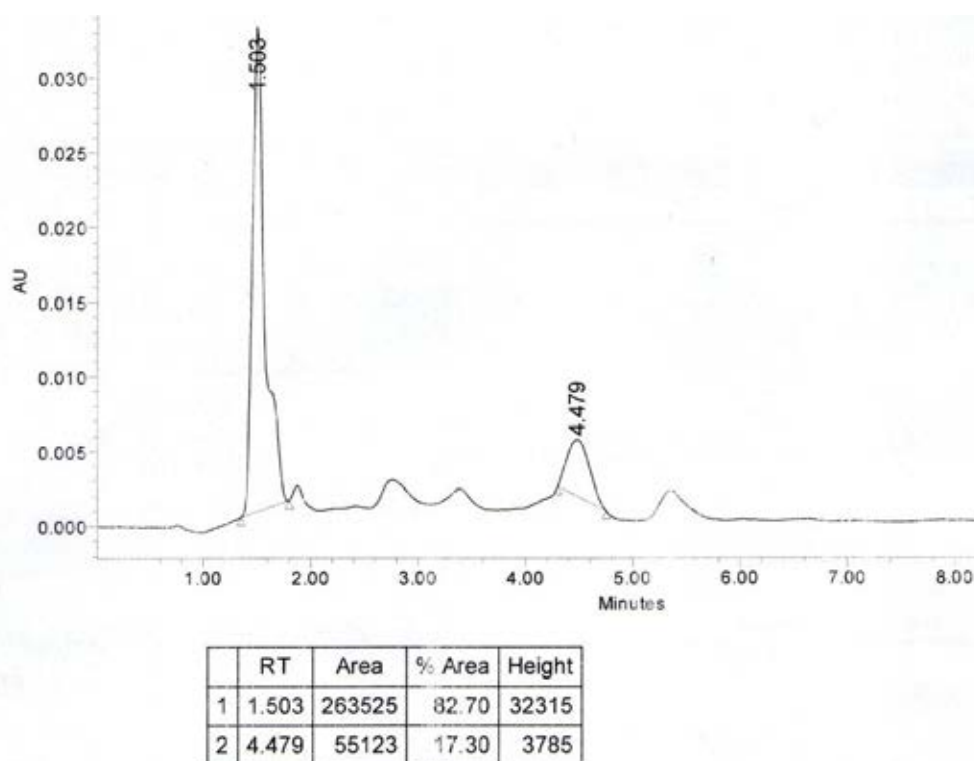
	RT	Area	% Area	Height
1	1.503	263525	82.70	32315
2	4.479	55123	17.30	3785

**Figure B1** HPLC chromatogram of remained AG solution

Preparation of andrographolide calibration curve

The experiment was done by dissolving 10 mg of AG with 50 mL of MeOH. This sample was use as stock solution and was further diluted to be the concentration of 100 to 900 μg/mL in test tubes. The area peak of each solution was determined by HPLC method using a reverse-phase ACE 5 C18-AR (150 mm × 4.6 mm) column and MeOH : H_2O (60 : 40) solvent system .

The area peak and standard calibration curve of AG were presented in Table B1 and Figure B2, respectively. The linear relation ship between concentration of AG and area showed acoefficient of determination curve (R^2) of 0.9985. This calibration curve was further used for calculating the amount of AG.

Table B1 The area peak of AG in MeOH solution

Concentration of AG (ppm)	Average Area of AG
0	0.00E+00
100	4.12E+06
300	1.16E+07
500	2.02E+07
700	2.92E+07
900	3.57E+07

Calibration Curve

$y = 40343x$
$R^2 = 0.9985$
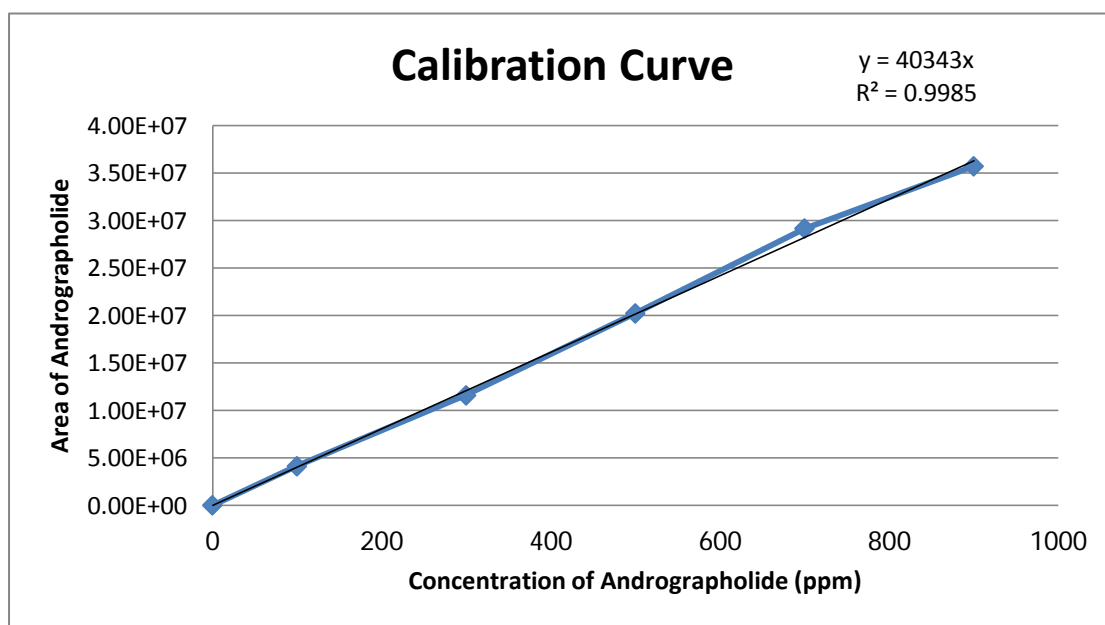
Figure B2 The calibration curve of peak area of andrographolide in MeOH

Appendix C

Fluorescene intensity of pyrene for Critical Aggregation Concentration (CAC) study

Table C1 The ratio of fluorescence emission intensity (I_{382}/I_{372}) and Log concentration of AGS-g-CS in distilled water

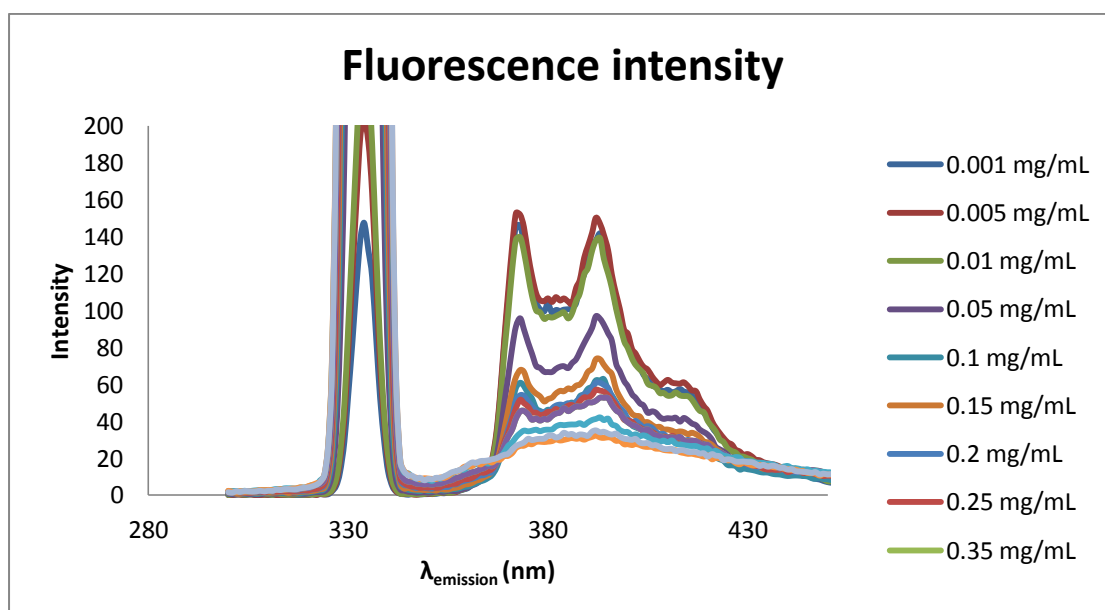| Concentration of AGS-*g*-CS (mg/mL)	log c	I_{382}/I_{372}
0.001	-3	0.689105
0.005	-2.30103	0.702364
0.01	-2	0.700508
0.05	-1.30103	0.748584
0.1	-1	0.821272
0.15	-0.82391	0.861833
0.2	-0.69897	0.945878
0.25	-0.60206	0.989822
0.35	-0.45593	1.066327
0.45	-0.34679	1.105244
0.7	-0.1549	1.18672
0.8	-0.09691	1.181672
1	0	1.171956

Figure C1 Fluorescene intensity of pyrene in various concentrations of AGS-g-CS solution

Appendix D

Dynamic Light Scattering (DLS)

Table D1 The dynamic light scattering data of AGS-*g*-CS in distilled water.

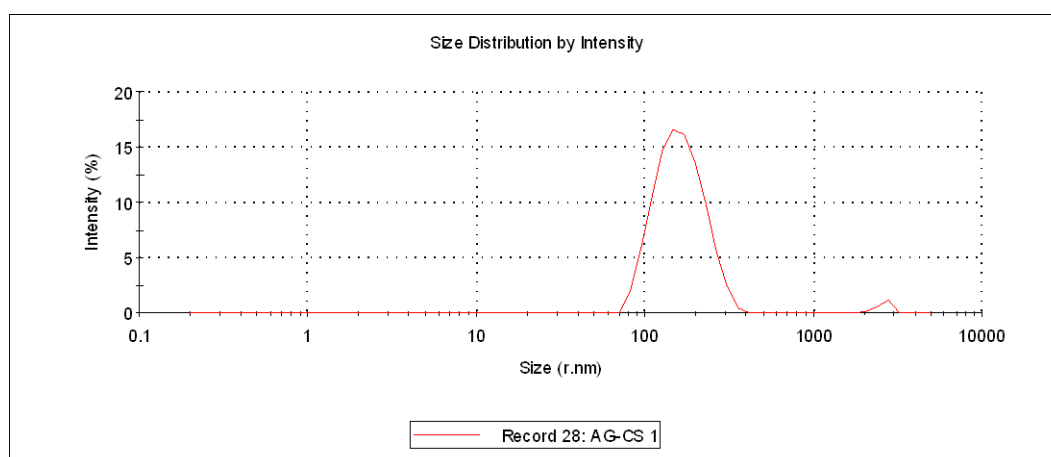| ample name	Hydrodynamic Diameter (nm)	Polydispersity Index	Zeta Potential (mV)
AGS-*g*-CS 1	155	0.226	39.80
AGS-*g*-CS 2	152	0.223	40.00
AGS-*g*-CS 3	155	0.233	41.20
Mean	154	0.227	40
SD	2	0.005	1

Figure D1 The size distribution graph of AG-*g*-NSCS 1
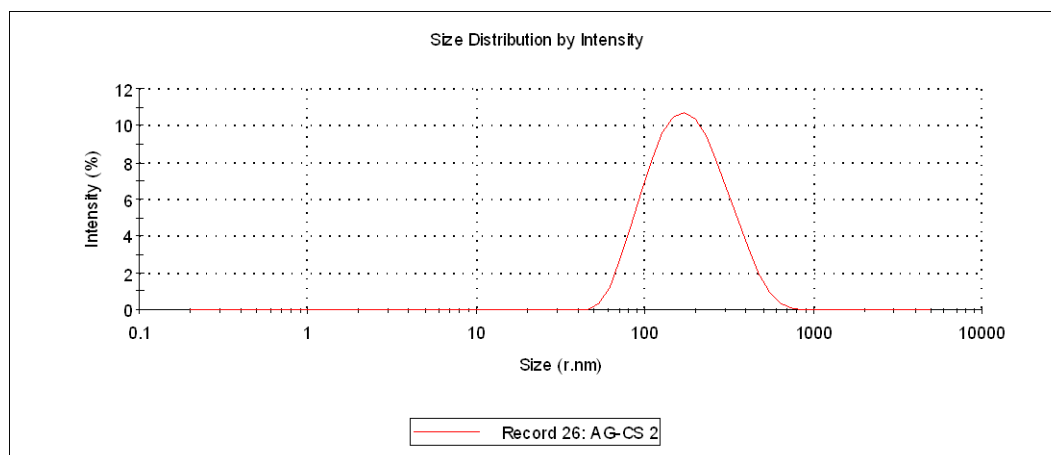
Figure D1 The size distribution graph of AGS-*g*-CS 2
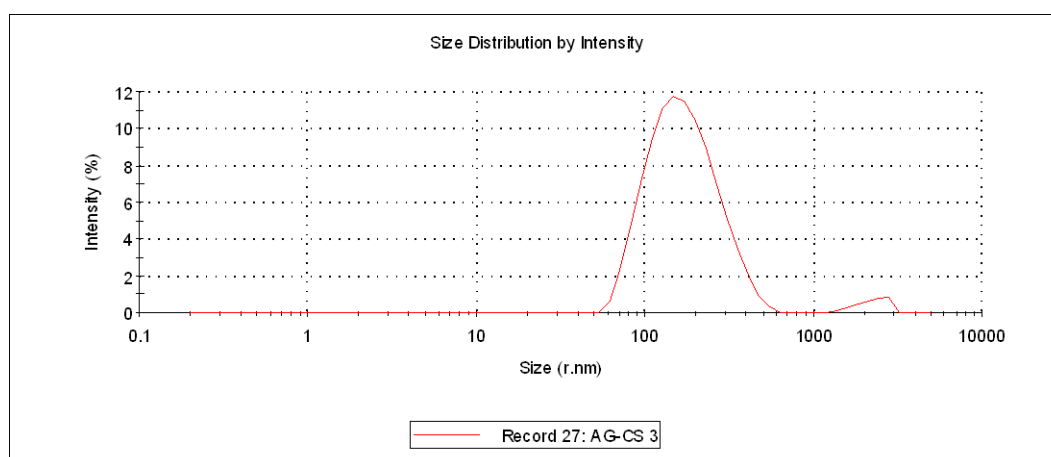
Figure D3 The size distribution graph of AGS-*g*-CS 3

VITAE

Name	:	Miss Siwaporn Srimongkol
Date of birth	:	October 29, 1987
Nationality	:	Thai
Address	:	72, Moo 4, Bangpa, Muang, Ratchaburi, 70000
University Education	:	Bachelor's Degree from Department of Material Science, Faculty of Engineer, Silpakorn University, 2006-2009
		Master's Degree from Program in Petrochemistry and Polymer Science, Faculty of Science, Chulalongkorn University
Conference attendance	:	Srimongkol, S.; Sawasdee, P. "A novel derivative of chitosan: andrographolide-*graft*-*N*-succinyl chitosan" The 8th Pure and Applied Chemistry International Conference 2013, The Tide resort, Chonburi, Thailand, 23-25 January 2013